Proposal

Measurement of High-Mass Dimuon Production at the 50-GeV Proton Synchrotron

April 28, 2006

J. Chiba[1], D. Dutta[2], H. Gao[2], Y. Goto[3], L. D. Isenhower[4], T. Iwata[11], S. Kato[11], M. J. Leitch[5], M. X. Liu[5], P. L. McGaughey[5], J. C. Peng[6†], P. Reimer[7], M. Sadler[4], N. Saito[8], S. Sawada[9†], T. -A. Shibata[10], K. H. Tanaka[9], R. Towell[4], and H. Y. Yoshida[11]

[1] *Department of Physics, Faculty of Science and Technology, Tokyo University of Science, Noda 278-8510, Japan*

[2] *Department of Physics, Duke University, Durham, NC 27708, USA*

[3] *RIKEN, Insitute of Physical and Chemical Research, Wako, Saitama 351-0198, Japan*

[4] *Department of Physics, Abilene Christian University, Abilene, TX 79699, USA*

[5] *Physics Division, LANL, Los Alamos, NM 87545, USA*

[6] *Department of Physics, University of Illinois at Urbana-Champaign, Urbana, IL 61801-3080, USA*

[7] *Physics Division, Argonne National Laboratory, Argonne, IL 60439-4843, USA*

[8] *Department of Physics, Kyoto University, Kyoto 606-8502, Japan*

[9] *High Energy Accelerator Research Organization, Ibaraki 305-0801, Japan*

[10] *Department of Physics, Tokyo Institute of Technology, Tokyo 152-8551, Japan*

[11] *Department of Physics, Yamagata University, Yamagata 990-8560, Japan*

[†]Co-spokespersons: J. C. Peng (jcpeng@uiuc.edu) and S. Sawada (shinya.sawada@kek.jp).

Abstract

We propose the construction of a spectrometer at J-PARC designed for the detection of high-mass dimuons produced in the interactions of 30 GeV and 50 GeV proton beams with various targets. Through the detections of the Drell-Yan, J/Ψ and Ψ', and single muon events, a broad physics program addressing various issues in QCD can be pursued. At the initial phase of 30 GeV running at J-PARC, the production and decay characteristics of J/Ψ and Ψ' can be studied. After the 50 GeV proton beam becomes available, unique measurements of the nucleon sea-quark flavor asymmetry and the antiquark contents in nuclei can be performed over the large Bjorken-x region of $0.25 < x < 0.6$. Furthermore, the effects of energy loss for fast quarks traversing nuclear medium could also be sensitively measured. Moreover, a rich program of spin-dependent structure function physics can be carried out through the measurements of unpolarized, singly polarized, and doubly polarized Drell-Yan processes. The construction and operation of this high-mass high-rate dimuon spectrometer at J-PARC will provide a unique tool to study quark nuclear physics complementary to the $p-p$, $p-A$, and $A-A$ programs at RHIC and the electron and muon scattering programs at JLab and at CERN.

Contents

1 Introduction

One of the most active areas of research in nuclear and particle physics during the last several decades is the study of quark and gluon distributions in the nucleons and nuclei. Several major surprises were discovered in Deep-Inelastic Scattering (DIS) experiments which profoundly changed our views of the partonic substructure of hadrons. In the early 1980's, the 'EMC' effect found in muon DIS provided the first unambiguous evidence that the quark distributions in nuclei are significantly different from those in free nucleons [1, 2]. More recently, surprising results on the spin and flavor structures of the nucleons were discovered in DIS experiments. Surprising results from the polarized DIS experiments have led to extensive theoretical and experimental efforts to understand the partonic content of proton's spin [3]. Subsequently, observation [4] of the violation of the Gottfried sum rule [5] in DIS revealed a surprisingly large asymmetry between the up and down antiquark distributions in the nucleon, shedding new light on the origins of the nucleon sea.

The partonic structure of nucleons and nuclei can also be measured with hadronic probes. A powerful tool for such studies is the Drell-Yan process [6], in which a quark annihilates with an antiquark forming a virtual photon which subsequently decays into a lepton pair. The proton-induced Drell-Yan process is of particular interest, since it can be used to extract antiquark distributions of the target nucleon and nuclei. This provides information complementary to what can be obtained in DIS, which is sensitive to the sum of the quark and antiquark distributions.

The usefulness of the Drell-Yan process as a tool for probing antiquark distributions has been well demonstrated by a series of Fermilab dimuon production experiments [7]. In particular, the Drell-Yan cross section ratios for $p + d$ versus $p + p$ led to a direct measurement of the $\bar{d}/\bar{u}$ asymmetry as a function of Bjorken-x [8, 9]. Furthermore, the nuclear dependence of the Drell-Yan cross sections showed no evidence for antiquark enhancement in heavy nuclei [10], in striking disagreements with predictions of some theoretical models which were capable of explaining the EMC effect.

The 50-GeV proton beam at J-PARC offers a unique opportunity to extend existing measurements of antiquark distributions to much larger values of Bjorken-x. Such information is crucial for understanding the origins of flavor asymmetry in the nucleon sea, and for illuminating the nuclear environment effects on sea-quark distributions.

A study of the nuclear dependence of Drell-Yan cross sections at 50 GeV would also provide a crucial test of the coherent partonic energy-loss effects predicted by Baier, Dokshitser, Mueller, Peigne, Schiff (BDMPS) [11] and by Zakharov [12]. The partonic energy-loss effect is the QCD analog of the Landau-Pomeranchuk-Migdal (LPM) QED effect [13, 14] predicted over 40 years ago and confirmed only in the 1990's at SLAC [15]. A number of surprising effects were obtained by BDMPS and Zakharov. First, the partonic energy loss in a hot QCD plasma is predicted to be much larger than in cold matter. This suggests that an anomalously large energy loss of jets could occur in relativistic heavy-ion collisions. Recent results from RHIC are supportive of this prediction. Second, the total radiative energy loss is predicted to be proportional to L^2, where L is the path length of the nuclear matter traversed by the partons. This striking prediction is contrary to the conventional wisdom that the total energy loss depends linearly on L, and it reflects the quantum-mechanical interference effect. This prediction remains to be tested by experiments.

Attempts to search for partonic energy-loss effects in cold matter have been made via the study of nuclear dependence of Drell-Yan cross sections at 800 GeV [16, 17] and via the nuclear effects of semi-inclusive DIS [18, 19]. However, the results from different measurements are not consistent [20]. A very sensitive measurement could be made at lower beam energies, where the fractional energy loss $\Delta E/E$ is relatively large. At the 50-GeV J-PARC, the effect is expected to be much enhanced and indeed the data could readily distinguish the L dependence from the L^2 dependence [20].

Detection of high-mass dileptons will also allow a study of J/Ψ and Ψ' production. Existing data on proton-induced charmonium production are mostly limited to the energy range 150 GeV $\leq E_p \leq$ 800 GeV. A comparison of charmonium production data at J-PARC energies with existing data will further improve our knowledge on the production and propagation of charmonium in the nuclear medium. Many different effects which could affect the production of charmonium in nuclear medium, such as nuclear shadowing, partonic energy loss, final-state interaction with comoving gluons or hadrons, will have different beam energy dependences [21, 22]. Therefore, a systematic study of charmonium production in $p-p$ and $p-A$ collisions at 30 GeV or 50 GeV would be extremely valuable for disentangling various effects. Only after the mechanisms for charmonium production are well understood could J/Ψ-suppression be used confidently as a signature for Quark-Gluon Plasma formation in relativistic heavy-ion collisions [23, 24].

Many of the proposed studies for Drell-Yan process at J-PARC could also benefit from the J/Ψ and Ψ' data. Unlike the Drell-Yan which is an electromagnetic process, quarkonium production is a strong-interaction process involving gluon-gluon fusion and quark-antiquark annihilation. Comparison between the Drell-Yan and quarkonium production data will further elucidate various aspects of parton distributions in nucleons and nuclei, and of the propagation of partons in nuclei. As an example, charmonium production with proton beam at J-PARC might provide interesting information on the gluon distributions at large Bjorken-x, which is essentially unknown.

The spin structure of the proton can also be investigated with the proposed dimuon spectrometer. In particular, polarzied Drell-Yan process with polarized beam and/or polarized target at J-PARC would allow a unique program on spin physics complementary to polarized DIS experiments and the RHIC-Spin program. Specific physics topics include the measurements of T-odd Boer-Mulders distribution function in unpolarized Drell-Yan, the extraction of T-odd Sivers distribution functions in singly transversely polarized Drell-Yan, and the helicity distribution of antiqaurks in doubly longitudinally polarized Drell-Yan. It is worth noting that polarized Drell-Yan is one of the major physics program at the GSI Polarized Antiproton Experiment (PAX). The RHIC-Spin program will likely provide the first results on polarized Drell-Yan. However, the high luminosity and the broad kinematic coverage for the large-x region at J-PARC would allow some unique measurements to be performed in the J-PARC dimuon experiments.

In the following sections, the physics motivations, the experimental approach, and proposed apparatus, and the expected results, are presented. The construction of the dimuon spectrometer at J-PARC would allow first measurements of J/Ψ and Ψ' production at the 30 GeV initial phase of J-PARC, followed by an extensive program on Drell-Yan, open-charm, and quarkonium productions at 50 GeV. The availability of polarized proton beam (and target) would further enrich the physics scope of the dimuon experiments in the future.

2 Physics Motivations for Dimuons at 50 GeV

2.1 Overview of high-mass dilepton production

Detection of high-mass dileptons produced in high-energy hadronic interactions has a long history. The charm and beauty quarks were discovered in the 1970's via the dilepton decay modes of J/Ψ and Υ resonances. These quarkonium states are superimposed on a dilepton continuum called the Drell-Yan process [6]. The Drell-Yan data has been a source of information for the antiquark structure of the nucleon [25].

To lowest order, the Drell-Yan process depends on the product of quark and antiquark distributions in the beam and target as

$$\frac{d^2\sigma}{dx_1 dx_2} = \frac{4\pi\alpha^2}{9s\ x_1 x_2} \sum_a e_a^2 [q_a(x_1)\bar{q}_a(x_2) + \bar{q}_a(x_1) q_a(x_2)]. \tag{1}$$

Here $q_a(x)$ are the quark or antiquark structure functions of the two colliding hadrons evaluated at momentum fractions x_1 and x_2. The sum is over the quark flavors a, and s is the center-of-mass energy squared. The kinematics of the virtual photon − longitudinal center-of-mass momentum $p_\parallel^\gamma$, transverse momentum p_T^γ and mass M_γ − are determined by measuring the two-muon decay of the virtual photon. These quantities determine the momentum fractions of the two quarks:

$$x_F = p_\parallel^\gamma / p_\parallel^{\gamma,max} = x_1 - x_2 \tag{2}$$

$$M_\gamma^2 = x_1 x_2 s \tag{3}$$

where $p_\parallel^\gamma$ is the virtual photon center-of-mass longitudinal momentum and $p_\parallel^{\gamma,max}$ is the maximum value it can have.

Although the simple parton model enjoyed considerable success in explaining many features of the early data, it was soon realized that QCD corrections to the parton model were required. The inclusion of the NLO diagrams for the Drell-Yan process brings excellent agreement between the calculations and the data. The mechanism for Drell-Yan process is now well understood theoretically, and quantitative information on the parton distributions can be reliably extracted via this process.

To gain sensitivity to the antiquark distribution of the target, one chooses a proton beam and selects the kinematic region of positive x_F and large x_1. In this limit the contribution from the second term in Eq. 1 is small and the first term is dominated by the $u(x_1)$ distribution of the proton. Under these circumstances, the ratio of the cross sections for two different targets, X and Y, which have A_X and A_Y nucleons is approximately the ratio of the $\bar{u}(x_2)$ distributions:

$$\frac{\frac{1}{A_X}\left(\frac{d\sigma^X}{dx_1 dx_2}\right)}{\frac{1}{A_Y}\left(\frac{d\sigma^Y}{dx_1 dx_2}\right)} \approx \left.\frac{\bar{u}^X(x_2)}{\bar{u}^Y(x_2)}\right|_{x_1 \gg x_2} \tag{4}$$

In this relation the cross sections are defined per nucleus but the parton distributions are conventionally defined per nucleon.

Eq. 4 demonstrates the power of Drell-Yan experiments in determining relative antiquark distributions. This feature was explored by recent Fermilab experiments using 800

GeV proton beams [7]. The 50-GeV proton beam at J-PARC provides a unique opportunity for extending the Fermilab measurements to larger x_2 ($x_2 > 0.25$). For a given value of x_1 and x_2, the Drell-Yan cross section is proportional to $1/s$ (see Eq. 1). Hence the cross section at 50 GeV is roughly 16 times greater than that at 800 GeV (The disadvantage at lower beam energies is that it has limited reach for small x_2, which could best be studied at higher beam energies). Furthermore, to the extent that the radiation dose scales as beam power, one can take ≈ 16 times higher beam flux at 50 GeV relative to 800 GeV. The combination of these two effects could lead to a two-orders-of-magnitude improvement in the statistics at high x_2 over previous Fermilab experiments.

2.2 $\bar{d}/\bar{u}$ at large x

For several decades following the discovery of partons in DIS experiment, it had been assumed that the distributions of $\bar{u}$ and $\bar{d}$ quarks were identical. Although the equality of $\bar{u}$ and $\bar{d}$ in the proton is not required by any known symmetry, this is a plausible assumption for sea quarks generated by gluon splitting. Because the masses of the up and down quarks are small compared to the confinement scale, nearly equal numbers of up and down sea quarks should result.

The assumption of $\bar{u}(x) = \bar{d}(x)$ can be tested by measurements of the Gottfried integral [5], defined as

$$I_G = \int_0^1 \left[F_2^p(x,Q^2) - F_2^n(x,Q^2)\right]/x \; dx = \frac{1}{3} + \frac{2}{3}\int_0^1 \left[\bar{u}_p(x) - \bar{d}_p(x)\right] dx, \tag{5}$$

where F_2^p and F_2^n are the proton and neutron structure functions measured in DIS experiments. Under the assumption of a symmetric sea, $\bar{u} = \bar{d}$, the Gottfried Sum Rule (GSR) [5], $I_G = 1/3$, is obtained. The most accurate measurement of the Gottfried integral, obtained by the New Muon Collaboration (NMC) [4], is 0.235 ± 0.026, significantly below 1/3. This surprising result strongly suggested that the assumption $\bar{u} = \bar{d}$ should be abandoned. Specifically, the NMC result implies

$$\int_0^1 \left[\bar{d}(x) - \bar{u}(x)\right] dx = 0.148 \pm 0.039. \tag{6}$$

Eq. 6 shows that only the integral of $\bar{d} - \bar{u}$ was deduced from the DIS measurements. The x dependence of $\bar{d} - \bar{u}$ remained unspecified.

The proton-induced Drell-Yan process provides an independent means to probe the flavor asymmetry of the nucleon sea [26]. An important advantage of the Drell-Yan process is that the x dependence of $\bar{d}/\bar{u}$ can be determined. The CERN experiment NA51 [27] first carried out a comparison of the Drell-Yan muon pair yield from hydrogen and deuterium using a 450 GeV/c proton beam. They found that at $\langle x \rangle = 0.18$ $\bar{u}/\bar{d} = 0.51 \pm 0.04 \pm 0.05$, showing a surprisingly large difference between the $\bar{u}$ and $\bar{d}$.

The Fermilab E866 experiment also measured the Drell-Yan muon pairs from 800-GeV/c protons interacting with liquid deuterium and hydrogen targets. Eq. 4 shows that the Drell-Yan cross section ratio at large x_F is approximately given as

$$\frac{\sigma_{DY}(p+d)}{2\sigma_{DY}(p+p)} \approx \frac{1}{2}\left(1 + \frac{\bar{d}(x_2)}{\bar{u}(x_2)}\right). \tag{7}$$

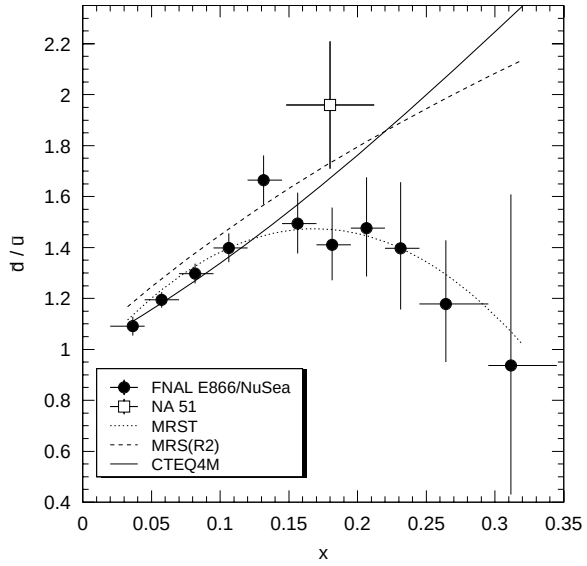

Figure 1: The ratio of $\bar{d}/\bar{u}$ in the proton as a function of x extracted from the Fermilab E866 [8] cross section ratio. The curves are from various parton distributions. Also shown is the result from NA51 [27], plotted as an open square.

Values for $\bar{d}/\bar{u}$ were extracted by the E866 collaboration at $Q^2 = 54$ GeV^2/c^2 over the region $0.02 < x < 0.345$. These are shown in Figure 1 along with the NA51 measurement. For $x < 0.15$, $\bar{d}/\bar{u}$ increases linearly with x and is in good agreement with the CTEQ4M [28] and MRS(R2) [29] parametrizations. However, a distinct feature of the data, not seen in either parametrization, is the rapid decrease toward unity of $\bar{d}/\bar{u}$ beyond $x = 0.2$.

The $\bar{d}/\bar{u}$ ratio, along with the CTEQ4M values for $\bar{d} + \bar{u}$, was used to obtain $\bar{d} - \bar{u}$ (Figure 2). Being a flavor nonsinglet quantity, $\bar{d}(x) - \bar{u}(x)$ is decoupled from gluon distribution. Since perturbative processes have negligible contribution to $\bar{d}/\bar{u}$ asymmetry, $\bar{d}(x) - \bar{u}(x)$ essentially isolates the contribution from non-perturbative effects.

Various theoretical models have been proposed to explain the $\bar{d}/\bar{u}$ asymmetry. In 1983, Thomas [30] pointed out that the virtual pions that dress the proton will lead to an enhancement of $\bar{d}$ relative to $\bar{u}$ via the (nonperturbative) "Sullivan process." Sullivan [31] showed that in DIS, virtual mesons scale in the Bjorken limit and contribute to the nucleon structure function. Following the publication of the NMC result, many papers [32] treated virtual mesons as the origin of the $\bar{d}/\bar{u}$ asymmetry (see [33, 34] for recent reviews). Here the $\pi^+(\bar{d}u)$ cloud, dominant in the process $p \to \pi^+ n$, leads to an excess of $\bar{d}$ sea.

A different approach for including the effects of virtual mesons has been presented by Eichten et al. [35] and further investigated by other authors [36, 37]. In chiral perturbation theory, the relevant degrees of freedom are constituent quarks, gluons, and Goldstone bosons. In this model, a portion of the sea comes from the couplings of Goldstone bosons to the constituent quarks, such as $u \to d\pi^+$ and $d \to u\pi^-$. The excess of $\bar{d}$ over $\bar{u}$ is then simply due to the additional valence u quark in the proton.

The flavor asymmetry of the nucelon sea has been computed in the large-N_c limit, where the nucleon is described as a soliton of an effective chiral theory [38, 39]. In this

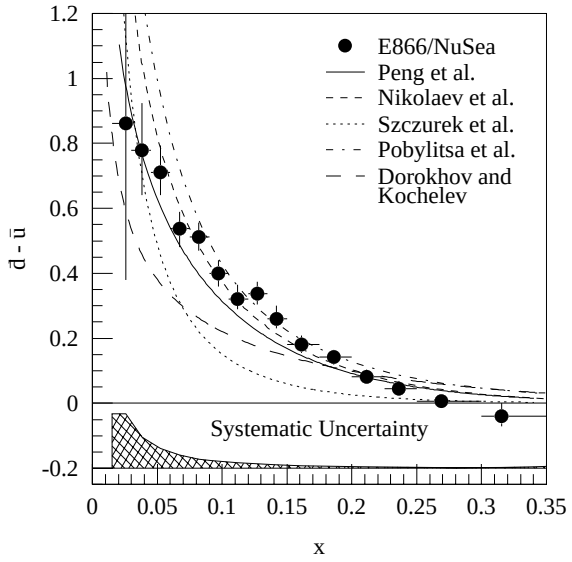

Figure 2: Comparison of the E866 [8] $\bar{d}-\bar{u}$ results at $Q^2 = 54$ GeV^2/c^2 with the predictions of various models.

chiral quark-soliton model, the flavor non-singlet distribution, $\bar{d}(x) - \bar{u}(x)$, appears in the next-to-leading order of the $1/N_c$ expansion [40]. Another interesting model relevant to the $\bar{d}/\bar{u}$ asymmetry is the instanton model. Instantons represent non-perturbative fluctuations of the gauge fields that induce transitions between degenerate ground states of different topology. The collision between a quark and an instanton flips the helicity of the quark while creating a $q\bar{q}$ pair of different flavor. The instanton model has the possibility of accounting for both the flavor asymmetry and the "spin crisis" [41, 42].

The x dependence of $\bar{d} - \bar{u}$ and $\bar{d}/\bar{u}$ obtained by E866 provides useful constraints for theoretical models. Figure 2 compares $\bar{d}(x) - \bar{u}(x)$ from E866 with various model calculations. The x dependence of the E866 data favors the virtual-pion model over the chiral model, suggesting that correlations between the chiral constituents should be taken into account. In general, most theoretical models are capable of describing the $\bar{d}(x) - \bar{u}(x)$ data from E866. However, the $\bar{d}(x)/\bar{u}(x)$ behavior at $x > 0.2$ are not described by any theoretical models. This is illustrated in Fig. 3, where the meson cloud model predicts a continuing rise in the $\bar{d}/\bar{u}$ at large x contrary to the trend exhibited in the data [43].

The interplay between the perturbative and non-perturbative components of the nucleon sea remains to be better determined. Since the perturbative process gives a symmetric $\bar{d}/\bar{u}$ while a non-perturbative process is needed to generate an asymmetric $\bar{d}/\bar{u}$ sea, the relative importance of these two components is directly reflected in the $\bar{d}/\bar{u}$ ratios. Thus, it would be very important to extend the Drell-Yan measurements to kinematic regimes beyond the current limits.

The 50-GeV proton beam at J-PARC presents an excellent opportunity for extending the $\bar{d}/\bar{u}$ measurement to larger x ($x > 0.25$). As mentioned earlier, for given values of x_1 and x_2 the Drell-Yan cross section is proportional to $1/s$, hence the Drell-Yan cross section at 50 GeV is roughly 16 times greater than at 800 GeV. Figure 4 shows the expected statistical accuracy for $\sigma(p+d)/2\sigma(p+p)$ at the 50-GeV J-PARC (see Section

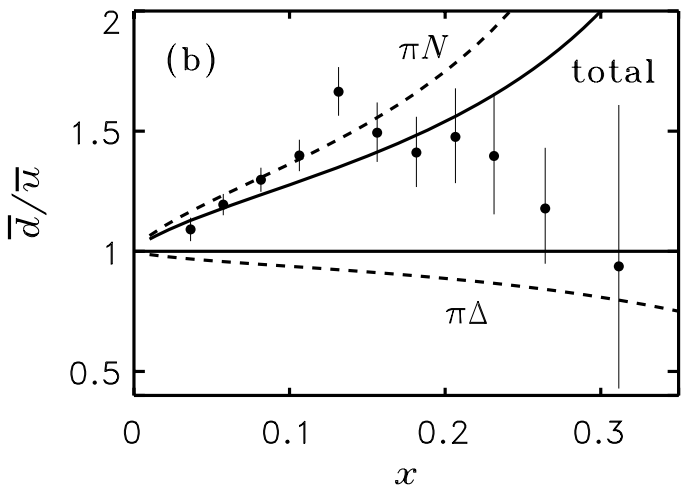

Figure 3: Comparison of the E866 [8] $\bar{d}/\bar{u}$ results at $Q^2 = 54$ GeV^2/c^2 with the predictions of meson cloud model [43]

5) compared with the data from E866 and a proposed measurement [44] using the 120 GeV proton beam at the Fermilab Main-Injector. A definitive measurement of the $\bar{d}/\bar{u}$ over the region $0.25 < x < 0.7$ could indeed be obtained at the 50-GeV J-PARC.

2.3 Quark energy loss in nuclei: Search for the LPM effet in QCD

The subject of energy loss of fast partons propagating through hadronic matters has attracted considerable interest recently [45]. One of the most exciting physics results to date at RHIC is the discovery of suppression of high transverse momentum pT $\sim$ 5-20 GeV mesons (jet candidates) in heavy ion collisions, interpreted in terms of medium-induced energy loss, predominantly via gluon bremsstrahlung emissions, of outgoing quarks and gluons (of initial energy $\sim$ 5-50GeV) in a high-density nuclear medium. This discovery is used as a cornerstone for the evidence that RHIC has produced a new state of matter (likely, QGP). However, this statement is undermined by the ambiguity over the correct approach to describing parton energy loss in terms of QCD. Several models, treating jet medium interactions through mutually inconsistent approximations, have been shown to successfully describe available data. As a result, translating the jet energy loss observation into a quantitative determination of the properties of the medium created at RHIC, such as an estimation of the initial partonic density or temperature, has been problematic, and it will remain so until we solve the ambiguity experimentally. Much of the above problem stems from the lack of a theoretical common agreement of the processes and mechanisms to be included in specifying the energy loss, and the inability to directly check them experimentally. In order to study QGP properties quantitatively with jet tomography, it is critical to understand high-energy parton energy loss in nuclear medium first.

The nuclear dependence of the Drell-Yan process provides a particularly clean way to

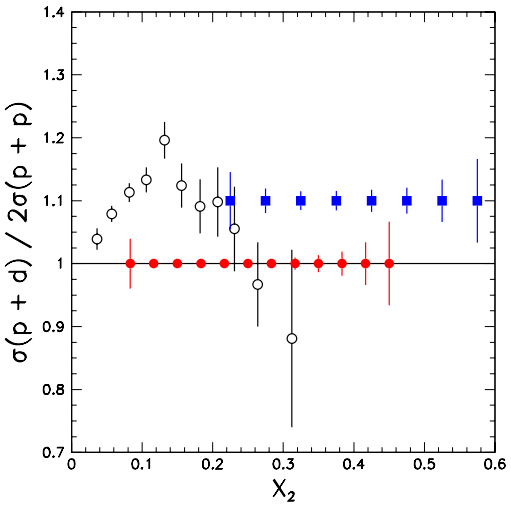

Figure 4: $(p+d)/(p+p)$ Drell-Yan ratios from E866 (open circles) are compared with the expected sensitivites at the 120 GeV Main Injector (solid circles) and the 50-GeV J-PARC (solid squares).

measure the energy loss of incident quarks in a cold nuclear medium. Partonic energy loss would lead to a degradation of the quark momentum prior to annihilation, resulting in a less energetic muon pair. Therefore, one expects the Drell-Yan cross sections for heavier nuclear targets to drop more rapidly at large x_1 (or x_F).

$$\frac{\delta\sigma^{DY}_{p+A}}{\delta\sigma^{DY}_{p+d}} \approx \frac{(1-x_1^A)^3}{(1-x_1^D)^3}. \tag{8}$$

Data from E772 at 800 GeV/c were analyzed by Gavin and Milana [46] to deduce the initial-state quark energy loss. They ignored the shadowing effect and assumed the following expression for the average change in the momentum fraction:

$$\Delta x_1 = -\kappa_1 x_1 A^{1/3}. \tag{9}$$

A surprisingly large fractional energy loss ($\approx 0.4\%/fm$) was obtained. This result was questioned by Brodsky and Hoyer [47], who argued that the time scale for gluon bremsstrahlung need to be taken into account. Moreover, as pointed out in Ref. [7], it is important to account for the shadowing effect before a reliable value of partonic energy loss can be extracted. Using an analogy to the photon bremsstrahlung process, Brodsky and Hoyer suggested an alternative expression:

$$\Delta x_1 \approx -\frac{\kappa_2}{s} A^{1/3}, \tag{10}$$

where s is the square of the nucleon-nucleon center-of-mass energy. Note that Eq. 9 implies a linear dependence of the energy loss on the partonic energy, while Eq. 10 assumes a constant energy loss independent of the partonic energy (note that ΔE is proportional

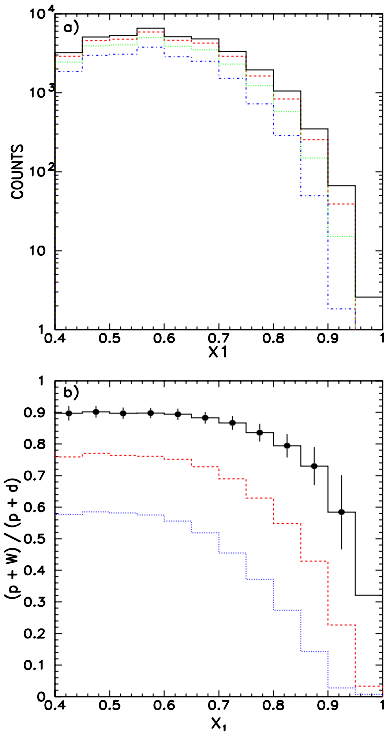

Figure 5: a): Solid curve is the expected $p+d$ spectrum for a 60-day run at 50 GeV. The dashed, dotted, and dash-dotted curves correspond to $p+W$ spectra assuming a partonic energy loss rate of 0.1, 0.25, 0.5 GeV/fm, respectively. b): Solid circles show the expected statistical errors for $(p+W)/(p+d)$ ratios in a 60-day run for $p+W$ and $p+p$ each. The solid, dashed, and dotted curves correspond to a partonic energy loss rate of 0.1, 0.25, 0.5 GeV/fm, respectively.

to $\Delta x_1 s$). Based on uncertainty principle, Brodsky and Hoyer concluded that energetic partons should loose ≤ 0.5 GeV/fm in nuclei. More recently, Baier et al. [11] and Zakharov [12] predicted

$$\Delta x_1 \approx -\frac{\kappa_3}{s} A^{2/3}. \tag{11}$$

These authors obtained the nonintuitive result that the total energy loss is proportional to the square of the path length traversed. Recently, the E866 nuclear-dependence data have been analyzed by taking into consideration the shadowing effect and comparing with the three different expressions (Eqs. 9 - 11) for energy loss [16]. Upper limits of $\kappa_2 < 0.75$ GeV^2 and $\kappa_3 < 0.10$ GeV^2 have been obtained. The κ_2 limit corresponds to a constant energy loss rate of < 0.44 GeV/fm, while the κ_3 limit implies $\Delta E < 0.046$ GeV/fm$^2 \times L^2$, where L is the quark propagation length through the nucleus. This is very close to the lower value given by Baier et al. [11] for cold nuclear matter.

A much more sensitive study of the partonic energy loss could be carried out at the 50-GeV J-PARC. We have simulated the effect of initial-state energy loss on the $p+W$ Drell-Yan cross sections, and the results [20] are shown in Figure 5. Assuming a 60-day run with the nominal spectrometer configuration (see Section 5), the expected x_1

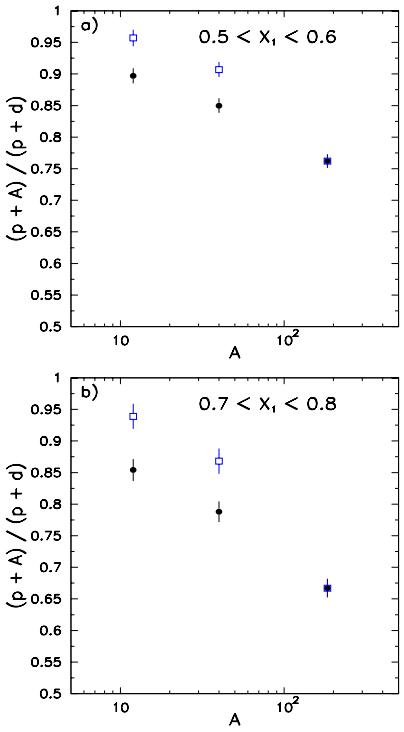

Figure 6: a): Solid circles correspond to the expected $(p + A)/(p + d)$ ratios assuming a partonic energy loss rate of 0.25 GeV/fm with a nuclear dependence given by Eq. 10. The open squares correspond to partonic energy loss given by Eq. 11. The statistical errors were calculated assuming a 60-day run for each target. b) Same as the top figure, but for a different x_1 bin $(0.7 < x < 0.8)$.

distribution for $p + d$ is shown as the solid curve. The dashed, dotted, and dash-dotted curves in Figure 5 correspond to $p + W$ x_1 spectra assuming a partonic energy loss form of Eq. 10 with dE/dz of -0.1, -0.25, -0.5 GeV/fm, respectively. The ratios of $p + W$ over $p+d$, shown in Figure 5, are very sensitive to the quark energy loss rate, and the expected statistical accuracy can easily identify an energy loss as small as 0.1 GeV/fm. The greater sensitivity at 50 GeV is due to the $1/s$ factor in Eq. 10 and Eq. 11. Another important advantage at 50 GeV is the absence of shadowing effect, and no shadowing correction is required.

A detailed study of the nuclear dependence of Drell-Yan cross-sections at 50GeV could also lead to a first observation of the coherent quark energy loss effects predicted recently by Baier et al. and Zakharov . The effects are the QCD analog of the Landau-Pomeranchuk-Migdal (LPM) QED effect predicted over 50 years ago and confirmed only recently at SLAC . One interesting effects from BDMPS is that the total radiative energy loss is predicted to be proportional to L^2 (as in Eq. 11). This curious result is contrary to the conventional wisdom that energy loss depends linearly on L (as in Eq. 10). This is illustrated in Figure 6, where the solid circles correspond to $(p + A)/(p + d)$ assuming an energy-loss rate of 0.25 GeV/fm using Eq. 10. The open squares correspond to the situation when energy loss is described by Eq. 11 (the value of κ_3 is selected by matching

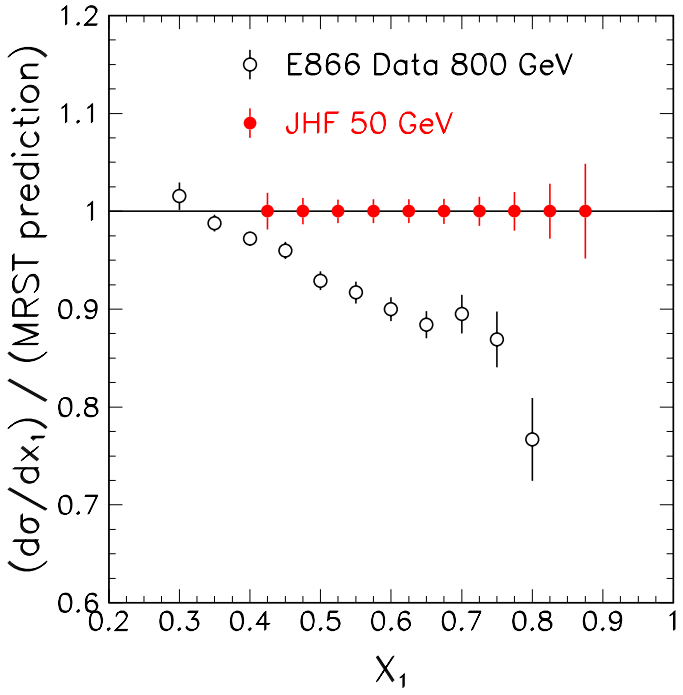

Figure 7: Ratios of the $d\sigma/dx_1$ data over the NLO calculation from E866. The expected statistical sensitivity of the J-PARC measurement is shown as the solid points.

the $(p+W)/(p+d)$ values for both cases). Figure 6 shows that one can easily distinguish an L- from an L^2-dependence even when the energy loss rate is as small as 0.25 GeV/fm.

2.4 u-quark distribution at large-x

A subject of much interest is the behavior of $d(x)/u(x)$ at large $x(x > 0.6)$. SU(6) symmetry predicts that $d/u \to 1/2$ at $x \to 1$, while QCD-inspired models predict that $d/u \to 1/5$ for the so-called $S_Z = 0$ dominance model [48] and $d/u \to 0$ for the $S = 0$ dominance model [49]. A precise measurement of $d(x)/u(x)$ at large x using various electron scattering processes is one of the major physics goals of the 12 GeV upgrade at the Jefferson Lab.

A precise measurement of the $u(x)$ distribution at large x is also of interest and would be relevant for the study of $d(x)/u(x)$ ratios. The $p+p$ and $p+d$ Drell-Yan cross sections are dominated by the $u(x_1)\bar{u}(x_2)$ term at large positive x_F. This shows that the Drell-Yan data at J-PARC would also be sensitive to the large-x behavior of the valence u-quark.

Recently, Fermilab E866 reported that the $p + p$ and $p + d$ Drell-Yan cross sections $d\sigma/dx_1$ appear to deviate significantly from the prediction of the NLO calculations using MRST structure functions [50], as shown in Fig. 7. This surprising result suggests that our current knowledge on the large-x u-quark distributions might be in question. Additional Drell-Yan data from J-PARC would be very important for determining the large-x u-quark distributions. Figure 7 shows the kinematic coverage in x_1 and the expected statistical

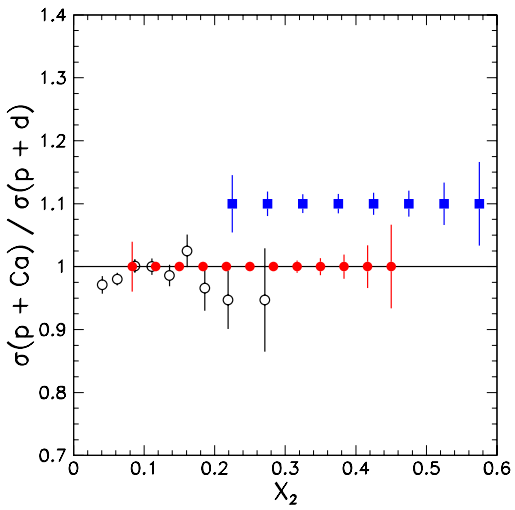

Figure 8: $(p + Ca)/(p + d)$ Drell-Yan ratios from E772 (open circles) are compared with the expected sensitivites at the 120-GeV Main Injector (solid circles) and at the 50-GeV PS (solid squares).

sensitivity for a two-month $p + d$ run with the proposed dimuon spectrometer.

2.5 Antiquark distributions in nuclei

Following the discovery of the EMC effect, it was suggested [51, 52, 53] that this effect is caused by the excess of virtual pions in nuclei, which significantly modify the nuclear parton distributions. A direct consequence of the "pion-excess" model is the nuclear enhancement of antiquark sea, which can be probed via Drell-Yan experiment [54]. However, the subsequent Fermilab E772 experiment [10] found no evidence for such enhancement (see Figure 8). The lack of an antiquark enhancement in nuclei suggests that there are no more pions surrounding an average nucleon in a heavy nucleus than there are in a weakly bound system, deuterium. This contradicts conventional wisdom and is also at odds with sophisticated calculations using realistic nuclear force [55]. Unfortunately, the error bars for the E772 data in the region $x > 0.15$ become quite large, due entirely to limited statistics. Furthermore, at $x < 0.1$ the on-set of the shadowing effect makes the isolation of possible pion-excess effect somewhat uncertain.

At the 50-GeV J-PARC, one can measure the nuclear effect over the large x region ($x > 0.15$) with high accuracy. This is illustrated in Figure 8, where the expected statistical errors for a 60-day measurement of $p + Ca$ and $p + d$ using the proposed spectrometer (see Section 5) are shown. One advantage of the 50-GeV measurement is that shadowing effect is no longer important at large x. The precise measurement at x larger than E772 could access would provide extremely valuable new information on the nuclear dependence of antiquark distributions. The anticipated sensitivity will be sufficient to observe the reduction in the nuclear sea distributions predicted in the Q^2 rescaling models [56]. The pion-excess model, on the other hand, predicts a strong nuclear enhancement of Drell-Yan

cross sections in this x region.

2.6 Boer-Mulder's functions via cos2ϕ distribution

A long-standing puzzle in pion-induced Drell-Yan data is the apparent violation of the Lam-Tung relation [57]. The decay angular distribution for Drell-Yan events can be described by the following general expression

$$\frac{1}{\sigma}\frac{d\sigma}{d\Omega} \sim 1 + \lambda \cos^2\theta + \mu \sin 2\theta \cos\phi + \frac{\nu}{2}\sin^2\theta \cos 2\phi, \tag{12}$$

where θ and ϕ are the polar and azimuthal decay angles in the dimuon rest frame (Collins-Soper or Gottfried-Jackson frame). The Lam-Tung relation, $1 - \lambda - 2\nu = 0$, is based on the spin-1/2 nature of the quark and is the Drell-Yan analog of the Callan-Gross relation in DIS. Existing pion-induced Drell-Yan data [58, 59] show that ν is sizable and the Lam-Tung relation is clearly violated. Nonperturbative effect, such as the pion bound state effect [60] can not explain the violation of the Lam-Tung relation.

Brandenburg and collaborators [61] suggested that the observed azimuthal cos2ϕ distribution is caused by the correlation between the quark transverse momentum and its transverse spin. More recently, Boer [62] suggested that the k_T-dependent parton distribution, $h_1^\perp$, would provide such a correlation. Boer also showed that the pion data on cos2ϕ could be described by a parametrization of the $h_1^\perp$ distribution function. The $h_1^\perp$ k_T-dependent distribution function has the interesting property that it is time-reversal odd. In the quark-diquark model, $h_1^\perp$ is identical to the T-odd Sivers function. It is predicted that both the Sivers function and the $h_1^\perp$ function obtained in the Drell-Yan process would have the same magnitude but with opposite sign compared to those obtained from DIS. This striking prediction remain to be tested experimentally.

There has been no measurement on the cos2ϕ distribution for proton-induced Drell-Yan. It is of great interest to check if the Lam-Tung relation is also violated in this case. Furthermore, these data could shed additional light on the origin for the large $\cos 2\phi$ azimuthal dependence observed in pion-induced Drell-Yan. One would expect that proton-induced Drell-Yan would have a much smaller azimuthal dependence, since the sea-quark $h_1^\perp$ is involved here. The proposed J-PARC dimuon experiment could provide a high statistics measurement of the cos2ϕ azimuthal dependence.

2.7 Quarkonium production at 50 GeV

Unlike the Drell-Yan process, the mechanisms for J/Ψ production are not well understood. Several quarkonium production models have been considered in the literature, including color-evaporation, color-singlet, and color-octet models. For simplicity, we consider the color-evaporation model, which is capable of describing the energy-dependence and the shape of the differential cross sections well. However, the absolute normalization of this model is treated as a parameter.

Figure 9 shows the prediction of the color-evaporation model for J/Ψ production at 50 GeV. The absolute normalization is obtained from an extrapolation of the global fit of existing J/Ψ data [63]. Unlike the situation at 800 GeV where the gluon-gluon fusion subprocess dominates [64], Figure 9 shows that the quark-antiquark annihilation is the dominant subprocess at 50 GeV. While this is reminiscent of the Drell-Yan process, it is

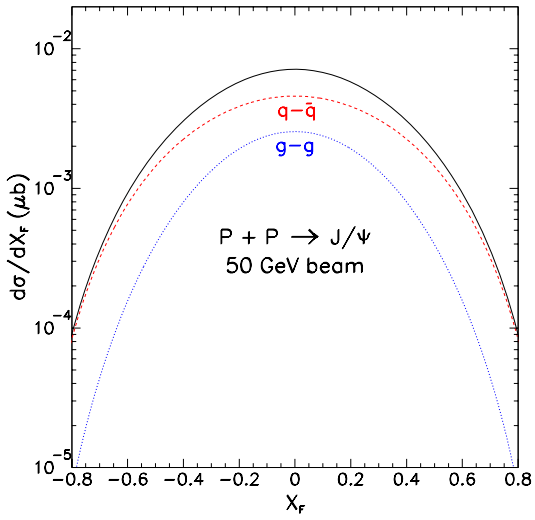

Figure 9: Calculation of the $p + d \rightarrow J/\Psi + x$ cross sections at 50 GeV using the color-evaporation model and the CTEQ5L structure functions. The contributions from the gluon-gluon fusion and the quark-antiquark annihilation subprocesses are also shown.

worth noting that quarkonium production is a hadronic process unlike the electromagnetic Drell-Yan process. Hence, there is no e_q^2 weighting factor for the $q - \bar{q}$ subprocess in J/Ψ production.

As indicated in Figure 9, the J/Ψ production data at 50 GeV are largely sensitive to quark distributions and could provide information similar to Drell-Yan. This is illustrated in Figure 10 which shows that the J/Ψ cross section ratio for $\sigma(p + d)/\sigma(p + p)$ is very sensitive to the $\bar{d}/\bar{u}$ asymmetry just like the Drell-Yan process. This could be readily tested at the 50-GeV J-PARC, since the J/Ψ event rate is expected to be very high.

Additional physics topics for J/Ψ and Ψ' production are discussed in the next Section.

3 Physics Motivations for Dimuons at 30 GeV

Since the first proton beam at J-PARC will be at 30 GeV, we expect that the initial measurements using the dimuon spectrometer will focus on J/Ψ and Ψ' production. In this Section, we outline the physics topics which can already be pursued for quarkonium production using 30 GeV proton beam.

3.1 J/Ψ production at 30 GeV

Using the parametrization of Ref. [63], one expects a reduction of the total cross section for J/Ψ production by a factor of ~ 5 when the beam energy is reduced from 50 GeV to 30 GeV. The calculation using the color-evaporation model and the CTEQ5L structure function is shown in Figure 11. As expected, the $q - \bar{q}$ annihilation process dominates the gluon-gluon fusion process at 30 GeV. This suggests that the J/Ψ cross section ratio for

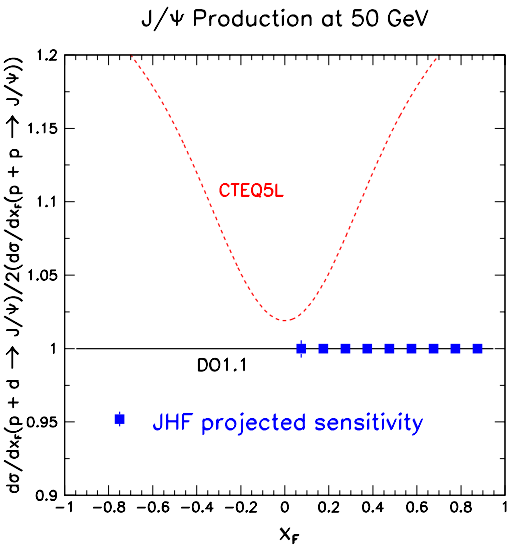

Figure 10: Calculations of the $p + d \rightarrow J/\Psi$ over $p + p \rightarrow J/\Psi$ ratios at 50 GeV using the color-evaporation model. The $\bar{d}/\bar{u}$-symmetric structure functions DO1.1 and the $\bar{d}/\bar{u}$ asymmetric structure functions (MRST and CTEQ4M) have been used in these calculations.

$p + d$ over $p + p$ is even more sensitive to the $\bar{d}/\bar{u}$ asymmetry than at 50 GeV as shown in Figure 12. The smaller cross sections at 30 GeV would not affect the statistical accuracy of the measurement, since the count rates for J/Ψ are high.

3.2 J/Ψ and Ψ' polarization

The production mechanisms of J/Ψ and Ψ' are still not completely understood despite some important recent progress. A new approach [65] based on nonrelativistic quantum chromodynamics (NRQCD) are capable of describing the production cross sections of J/Ψ and Ψ' at collider energies. This approach finds that the color-octet contributions dominate the cross sections. Further tests of the NRQCD include the polarization of the J/Ψ and Ψ', which are very sensitive to the color-spin states of the intermediate $c\bar{c}$ states. Recently, a high statistics measurement of the J/Ψ polarization in 800 GeV p-Cu interaction [66] showed that the polarization of is small but nonzero. The J/Ψ polarization has an interesting x_F dependence, being unpolarized at small x_F and becoming longitudinally polarized at large x_F. The size of the J/Ψ polarization is in disagreement with the prediction of a NRQCD calculation [67]. The measurement of J/Ψ polarization at 30 GeV could provide valuable information on the beam energy dependence of the J/Ψ polarization.

No data exist for the polarization of Ψ' at fixed-target energies. The measurement of Ψ' polarization is of considerable interest since a recent measurement [68] of 800 GeV p+Cu Υ resonances polarizations showed the surprising result that $\Upsilon(1S)$ is unpolarized while $\Upsilon(2S + 3S)$ has a large transverse polarization. At 30 GeV, the expected statistics and kinematic coverage would allow a very accurate measurement of the J/Ψ as well as

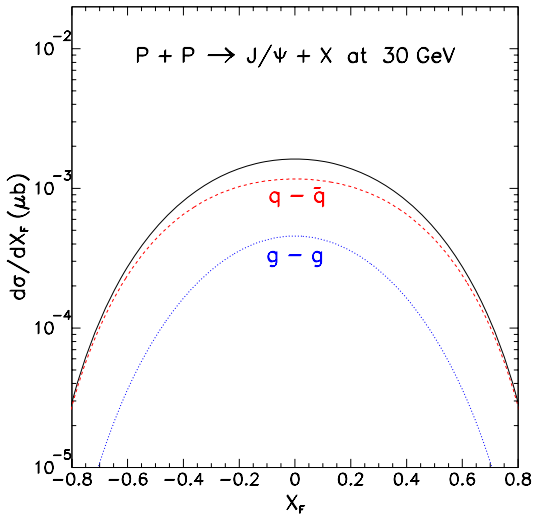

Figure 11: Calculation of the $p + d \rightarrow J/\Psi + x$ cross sections at 30 GeV using the color-evaporation model and the CTEQ5L structure functions. The contributions from the gluon-gluon fusion and the quark-antiquark annihilation subprocesses are also shown.

the Ψ' polarization. It would be very interesting to check if Ψ' is also strongly polarized just like the $\Upsilon(2S + 3S)$ resonances. The measurement of J/Ψ polarization could also provide valuable insight on the beam energy dependence of the J/Ψ polarization.

3.3 Nuclear effects of J/Ψ and Ψ' productions

Detailed nuclear dependences of J/Ψ and Ψ' production have been studied in $p + A$ collision at 800 GeV/c [69]. Striking p_T and x_F dependences have been observed, as shown in Figure 13 and Figure 14. Since the gluon-gluon fusion process dominates the quarkonium production at 800 GeV while at 30 GeV the $q\bar{q}$ annihilation is the primary mechanism, one expects that the nuclear effects at 30 GeV would be different from 800 GeV/c. We will have the opportunity to measure the nuclear effects of J/Ψ as well as the Ψ' production at J-PARC. With a two-month $p + W$ run, the expected sensitivity of the nuclear dependence parameter α is shown in Figure 13 and Figure 14.

4 Physics Motivations for Dimuons with Polarized Proton Beam

One of the key topics in hadron physics is to understand the spin structure of the nucleon. The nucleon's spin is a sum of contributions from the spin of the quark/antiquark ($\Delta\Sigma$), the spin of the gluon (ΔG), and the orbital angular momenta of the quark/antiquark and the gluon:

$$\frac{1}{2} = \frac{1}{2}\Delta\Sigma + \Delta G + L. \tag{13}$$

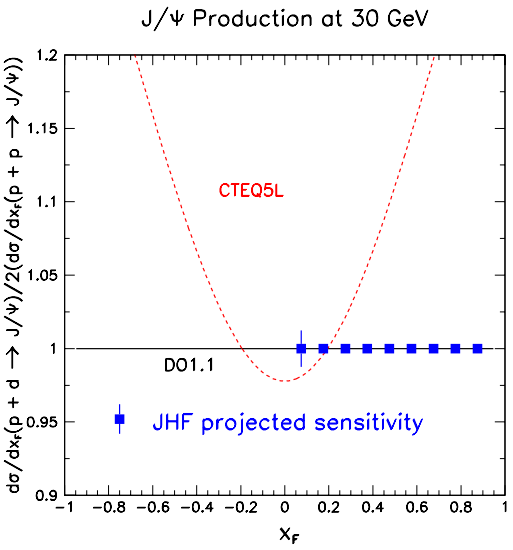

Figure 12: Calculations of the $p + d \rightarrow J/\Psi$ over $p + p \rightarrow J/\Psi$ ratios at 30 GeV using the color-evaporation model. The $\bar{d}/\bar{u}$-symmetric structure functions DO1.1 and the $\bar{d}/\bar{u}$ asymmetric structure function (CTEQ5L) have been used in these calculations.

In previous and current lepton DIS experiments, $\Delta\Sigma$ has been measured and found to contribute only 20-30% of the nucleon. Naively, it had been thought that the major fraction of the nucleon spin would come from $\Delta\Sigma$, and the discovery of this small contribution was called the spin puzzle. In order to solve the spin puzzle, lepton DIS and hadron collider experiments are actively measuring ΔG. The lepton DIS experiments (e.g. COMPASS experiment at CERN) are measuring ΔG by semi-inclusive hadron production. The hadron collider experiments (RHIC experiments at BNL) are measuring ΔG via double-helicity asymmetries of inclusive pions, jets, direct photons, etc. The remaining component to be measured is L, the orbital angular momenta of the quark/antiquark and the gluon.

In hadron experiments like that with a J-PARC primary beam, there is no clear way how to measure L. We have just hints from previous hadron experiments. In the Fermilab E704 experiment which is a fixed-target experiment with 200-GeV polarized proton and antiproton beams, it was observed that there is a large single transverse-spin asymmetry (A_N) in pion production in the forward rapidity region. In the naive picture of the QCD, A_N was estimated to be $\sim m_q/\sqrt{s}$ and very small. To explain the large observed A_N, many theoretical explanations are available now:

- Sivers effect
- higher-twist effect
- Collins effect (combined with the transversity distribution)

where the Sivers effect and the higher-twist effect are related to emitted gluons from initial-state hadron and correlation with gluons inside the hadron, and these effects are related to the transverse motion, or orbital angular motion, of partons inside the hadron.

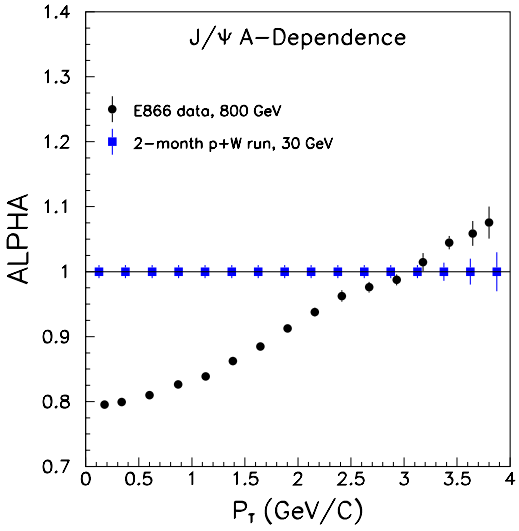

Figure 13: Expected statistical accuracy for measuring the nuclear dependence parameter α for a two-month $p+W$ measurement using 30 GeV proton beam at J-PARC. Data from the 800 GeV measurement are also shown.

It is important now to identify contribution of each mechanism. In order to disentangle these effects, many experimental data have been taken and many future experiments are planned. One of the most clear measurements is a Drell-Yan measurement at the hadron facilities. The Drell-Yan process is not affected by the final-state and free from Collins effect. Another method is A_N measurements of open charm production (D-meson, etc.) or bounded charm production (J/ψ, etc.).

In the Drell-Yan single transverse-spin measurement of A_N, or the $\sin(\phi-\phi_S)$ term, we can probe the Sivers effect and higher-twist effect. Here, ϕ is an azimuthal angle between the quark-antiquark plane and lepton plane defined in the Collins-Soper frame, and ϕ_S is the azimuthal angle of the proton polarization. This is discussed in subsection 4.1.

The $\sin(\phi+\phi_S)$ term of the Drell-Yan transverse-spin measurement gives the Boer-Mulders function combined with the transversity distribution. The transversity distribution, $h_1(x)$, is a parton distribution function (PDF) of the transverse spin of a parton inside the transversely polarized proton. The Boer-Mulders function, $h_1^\perp(x, \boldsymbol{k}_T)$, is a k_T-dependent T-odd PDF which a correlates the transverse-spin with the transverse momentum direction of a parton inside an unpolarized proton. The Boer-Mulders function can lead to a $\cos(2\phi)$ term of the unpolarized Drell-Yan measurement, and the transversity distribution can be measured in the Drell-Yan double transverse-spin asymmetry (A_{TT}). These are discussed in subsection 4.2.

A measurement of the quark and antiquark helicity distributions with longitudinally polarized beam and target (A_{LL} measurement) is discussed in subsection 4.3. A single spin asymmetry (SSA) measurement of charm production using a transversely polarized beam or target is discussed in subsection 4.4. A gluon polarization measurement using longitudinally polarized beam and target in charmonia production is discussed in subsection 4.5.

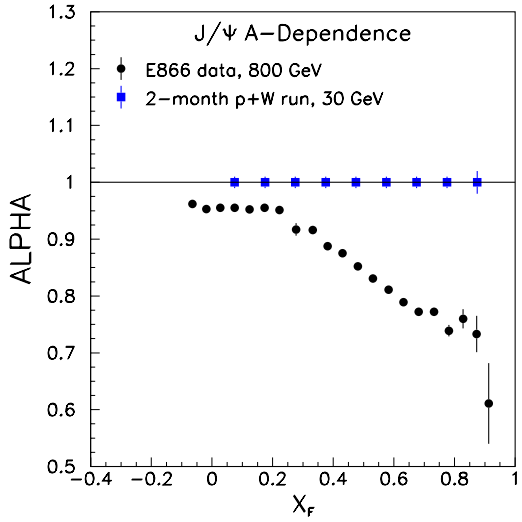

Figure 14: Expected statistical accuracy for measuring the nuclear dependence parameter α for a two-month $p+W$ measurement using 30 GeV proton beam at J-PARC. Data from the 800 GeV measurement are also shown.

4.1 Sivers effect and higher-twist effect with transversely polarized beam

The Sivers effect and the higher-twist effect generate a single spin asymmetry (SSA), A_N, in Drell-Yan lepton-pair production. Figure 15 shows the A_N integrated over q_T at $4 < M_{\mu^+\mu^-} < 5$ GeV calculated with Sivers function [70, 71] from HERMES data fit [72].

In Drell-Yan production at transverse momentum q_T and pair's mass Q, when q_T, $Q \gg \Lambda_{QCD}$, the higher-twist effect is applicable to calculate A_N. On the other hand, when $q_T \ll Q$, Sivers effect calculation can be applied. Therefore, in the intermediate region of q_T, $\Lambda_{QCD} \ll q_T \ll Q$, both effects should be applied and yield the same results [70].

4.2 Transversity and Boer-Mulders function with transversely polarized beam and/or target

By using both the transversely polarized beam and target, the transversity distribution are measured in the double transverse-spin asymmetry (A_{TT}) measurement of the Drell-Yan process [73].

$$A_{TT} = \hat{a}_{TT} \cdot \frac{\sum_q e_q^2(\bar{h}_{1q}(x_1)h_{1q}(x_2) + (1 \leftrightarrow 2))}{\sum_q e_q^2(\bar{f}_{1q}(x_1)f_{1q}(x_2) + (1 \leftrightarrow 2))} \tag{14}$$

where

$$\hat{a}_{TT} = \frac{\sin^2\theta \cos(2\phi - \phi_{S_1} - \phi_{S_2})}{1 + \cos^2\theta} \tag{15}$$

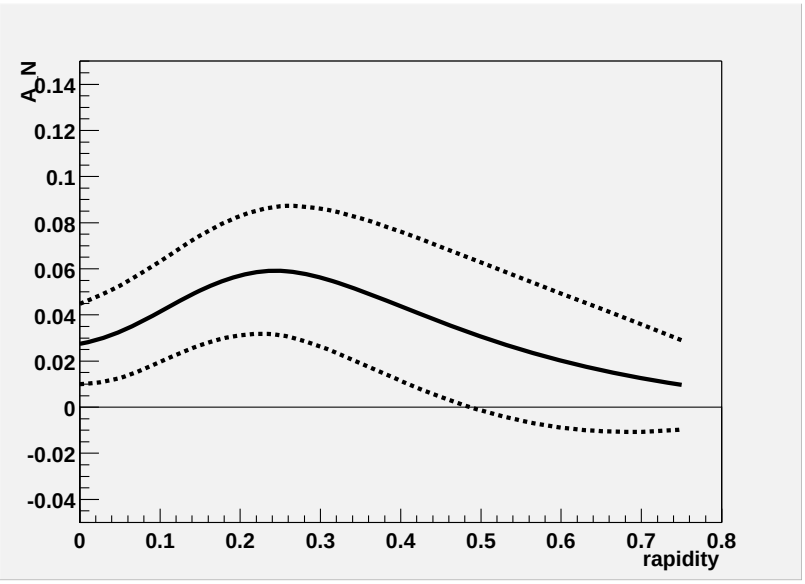

Figure 15: Drell-Yan A_N integrated over q_T at $4 < M_{\mu^+\mu^-} < 5$ GeV calculated with Sivers function from HERMES data fit.

and has an azimuthal distribution of $\cos(2\phi - \phi_{S_1} - \phi_{S_2})$.

By using either of the transversely polarized beam or target, the $\sin(\phi + \phi_S)$ term of the single transverse-spin measurement gives the transversity distribution combined with the Boer-Mulders function [74]. $\boldsymbol{q}_T$ (transverse momentum of virtual photon)-weighted single spin asymmetry is defined:

$$\hat{A} \equiv \frac{\int d\Omega d\phi_S \int d^2\boldsymbol{q}_T \frac{|\boldsymbol{q}_T|}{M_p} \sin(\phi + \phi_S)[d\sigma(\boldsymbol{S}_T) - d\sigma(-\boldsymbol{S}_T)]}{\int d\Omega d\phi_S \int d^2\boldsymbol{q}_T [d\sigma(\boldsymbol{S}_T) - d\sigma(-\boldsymbol{S}_T)]} \tag{16}$$

and it gives:

$$\hat{A} = -\frac{1}{2} \frac{\sum_q e_q^2 (\bar{h}_{1q}^{\perp(1)}(x_1) h_{1q}(x_2) + (1 \leftrightarrow 2))}{\sum_q e_q^2 (\bar{f}_{1q}(x_1) f_{1q}(x_2) + (1 \leftrightarrow 2))}. \tag{17}$$

The Boer-Mulders function can also be measured in the $\cos(2\phi)$ term of the unpolarized Drell-Yan measurement [74]. $\boldsymbol{q}_T$-weighted angular distribution is defined:

$$\hat{R} \equiv \frac{\int d^2\boldsymbol{q}_T \left(\frac{|\boldsymbol{q}_T|}{M_p}\right)^2 \frac{d\sigma^{(0)}}{d\Omega}}{\int d^2\boldsymbol{q}_T \sigma^{(0)}} \tag{18}$$

and parametrized as:

$$\hat{R} = \frac{3}{16\pi}(\gamma(1 + \cos^2\theta) + \hat{k}\cos 2\phi \sin^2\theta). \tag{19}$$

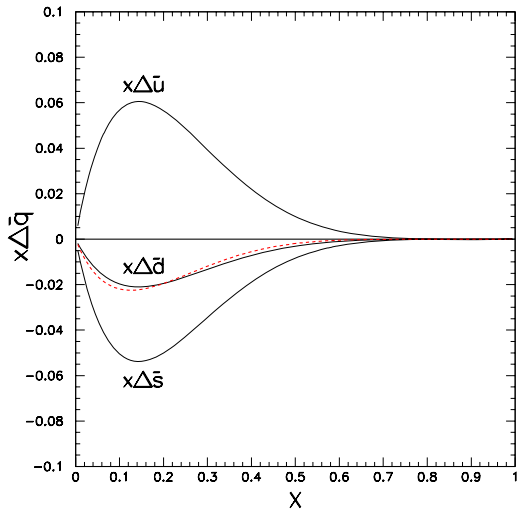

Figure 16: Sea quark polarizations at Q^2=0.36 GeV^2 predicted by chiral-quark soliton model are shown as solid curves. The dashed curve corresponds to the parametrization of $x\Delta\bar{q}$ at $Q^2 = 0.4\text{GeV}^2$ by GRSV, where $\Delta\bar{q} = \Delta\bar{u} = \Delta\bar{d} = \Delta\bar{s}$.

The coefficient $\hat{k}$ at the $\cos 2\phi$-dependent part gives:

$$\hat{k} = 8\frac{\sum_q e_q^2(\bar{h}_{1q}^{\perp(1)}(x_1)h_{1q}^{\perp(1)}(x_2) + (1 \leftrightarrow 2))}{\sum_q e_q^2(\bar{f}_{1q}(x_1)f_{1q}(x_2) + (1 \leftrightarrow 2))} \tag{20}$$

where

$$h_{1q}^{\perp(n)} \equiv \int d^2\boldsymbol{k}_T \left(\frac{\boldsymbol{k}_T^2}{2M^2}\right)^n h_{1q}^{\perp}(x, \boldsymbol{k}^2) \tag{21}$$

for the nth moment of the k_T-dependent PDF.

4.3 Quark and antiquark helicity distributions with longitudinally polarized beam and target

Despite extensive work on polarized DIS, the helicity distributions of $\bar{u}$ and $\bar{d}$ sea quarks are still poorly known. Both the SMC [75] and the HERMES [76] experiments attempted to extract the sea-quark polarizations via semi-inclusive polarized DIS measurements, and the results indicate small sea-quark polarization consistent with zero. However, as pointed out in Ref. [77], large uncertainties are associated with certain assumptions made in the extraction.

A direct measurement of sea-quark's polarization is clearly very important for understanding the flavor decomposition of proton's spin. Different theoretical models make drastically different predictions. In particular, the meson-cloud models, which successfully

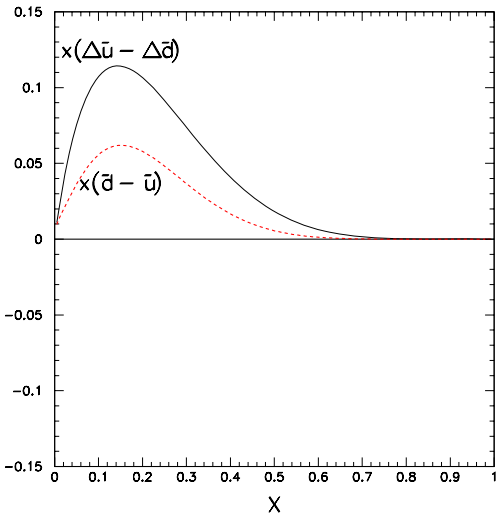

Figure 17: $x(\Delta\bar{u} - \Delta\bar{d})$ at $Q^2 = 0.36$ GeV^2 predicted by the chiral-quark soliton model is shown as the solid curve. The GRV94 LO parametrization of $x(\bar{d} - \bar{u})$ at $Q^2 = 0.4$ GeV^2 is shown as the dashed curve.

describe the unpolarized $\bar{d}/\bar{u}$ asymmetry, predict negligible amount of sea-quark polarization [78, 79]. Several current parametrizations [80, 81] of polarized parton distributions also assume very small polarization for sea quarks. The chiral-quark soliton model, on the other hand, predicts substantial sea-quark polarization [40, 77]. Figure 16 shows $x\Delta\bar{u}(x)$, $x\Delta\bar{d}(x)$, and $x\Delta\bar{s}(x)$ at $Q_0^2 = 0.36$ GeV^2 from a recent prediction of chiral-quark soliton model [82]. Also shown in Figure 16 are the GRSV parametrizations [81] from a global fit to polarized DIS data.

A very striking prediction of the chiral-quark model is the large flavor asymmetry of polarized sea-quark polarization. In fact, this model predicts a significantly larger values for $\Delta\bar{u} - \Delta\bar{d}$ than for $\bar{d} - \bar{u}$. This is shown in Figure 17, where $x(\Delta\bar{u} - \Delta\bar{d})$ from the chiral-quark soliton model [82] is compared with the $x(\bar{d} - \bar{u})$ parametrization from GRV94 [83].

Polarized proton beam at the 50-GeV PS would offer an exciting opportunity for probing sea-quark polarizations. The longitudinal spin asymmetry in the DY process is, in leading order, given by [84],

$$A_{LL}^{DY}(x_1, x_2) = \frac{\sum_a e_a^2[\Delta q_a(x_1)\Delta\bar{q}_a(x_2) + \Delta\bar{q}_a(x_1)\Delta q_a(x_2)]}{\sum_a e_a^2[q_a(x_1)\bar{q}_a(x_2) + \bar{q}_a(x_1)q_a(x_2)]}, \tag{22}$$

with $\Delta q_a \equiv q_a^+ - q_a^-$. The superscripts refer to parton spin projections parallel (+) or antiparallel (−) to the proton's spin projection. We have simulated the performance of the proposed high-mass dimuon spectrometer for measuring polarized antiquark distribution. Figure 18 shows the x_2 dependence of A_{LL}^{DY}, integrated over the spectrometer acceptance, for polarized sea-quark parametrizations including Gehrmann-Stirling (G-S) sets A and C [80] and GRSV Leading-Order set [81]. Very small values for A_{LL}^{DY} are predicted for the G-S parametrization, while the GRSV parametrization gives $A_{LL}^{DY} \approx -0.2$. The chiral-

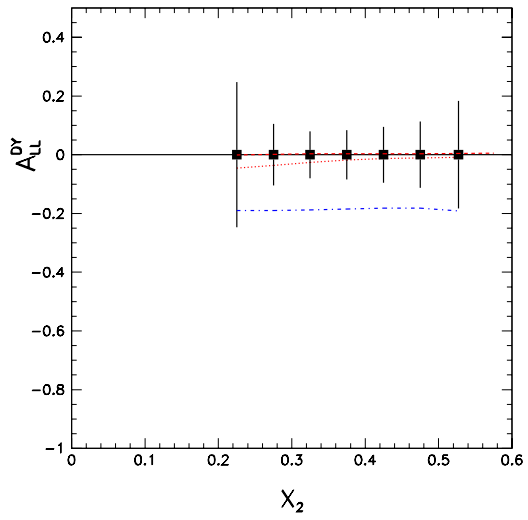

Figure 18: Expected statistical accuracy for measuring the double-helicity asymmetry A_{LL}^{DY} in polarized p+p Drell-Yan at the 50-GeV PS for a 120-day run. The dashed, dotted, and dash-dotted curves correspond to calculations using polarized PDF parametrization of G-S (set A, set C) and GRSV, respectively.

quark soliton model gives large positive A_{LL}^{DY}. In fact, the positivity requirement, namely, $-1 < \Delta\bar{u}(x)/\bar{u}(x) < 1$, is not always satisfied at the region $x > 0.2$ for the particular parametrization given by Ref. [82].

We have calculated the expected statistical sensitivities for a 120-day $\vec{p}+\vec{p}$ measurement, assuming 75% polarization for a 5×10^{11} per spill polarized proton beam. We also assume a polarized solid NH_3 target similar to the one used by the SMC [85] which achieves a hydrogen polarization of 75% and a dilution factor of 0.15. The target length is chosen to give the same gm/cm^2 as for the liquid deuterium target. Figure 18 shows that the statistical accuracy of such a measurement can well test the predictions of various model (note that the chiral-quark soliton model predicts a large positive A_{LL}^{DY} not shown in this figure). A comparison of $\vec{p}+\vec{p}$ with $\vec{p}+\vec{d}$ will further determine $\Delta\bar{d}$, which provides a direct test of the chiral-quark soliton model's prediction of large $\Delta\bar{u} - \Delta\bar{d}$.

4.4 Single spin asymmetry of charm production with transversely polarized beam or target

The charm production measured with transversely polarized beam or target gives us information on the Sivers distribution functions. In collider energies, it is dominated by the gluon-fusion process $gg \to c\bar{c}$ and has contributions from the quark-antiquark pair annihilation process $q\bar{q} \to c\bar{c}$ only at the large x_F region. In both processes there is no single spin transfer, so that the final c or $\bar{c}$ quarks are not polarized. Therefore, any SSA observed in the charm production cannot originate from the Collins fragmentation mechanism, but only from the Sivers effect in the distribution function. In particular, any sizable spin asymmetry measured at midrapidity will be a direct indication of a nonzero

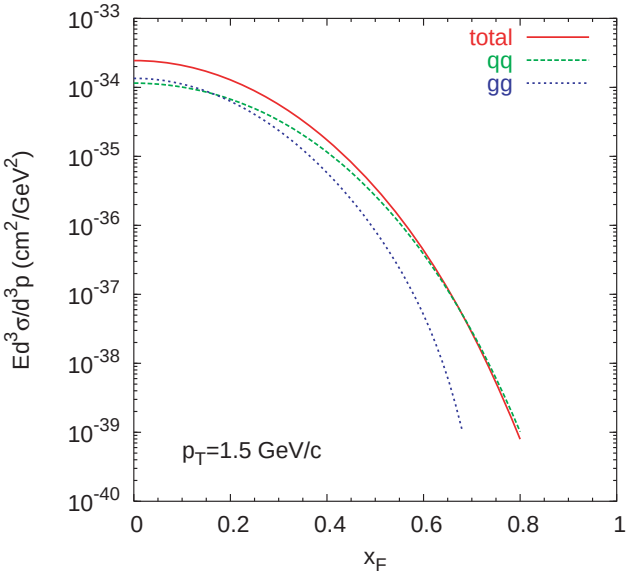

Figure 19: Invariant cross section of D-meson production and contributions from both the gluon fusion and quark-antiquark pair annihilation processes on it [86, 87].

Sivers gluon distribution function [86].

On the other hand, in J-PARC fixed-target experiment energies, contributions from the gluon-fusion process is much smaller. The SSA measurement is more sensitive to the Sivers quark distribution via the quark-antiquark pair annihilation process. The measurement is complimentary to the collider-energy measurements. Figure 19 shows a x_F spectrum of invariant cross section of D-meson production and contributions from both the gluon fusion and quark-antiquark pair annihilation processes on it. Figure 20 shows a A_N of D-meson production [87].

In the J-PARC energies which are closer to the threshold energy of the charm production, other processes, e.g. intrinsic charm production, may enhance the charm production cross section. Although other processes will dilute the sensitivity for the Sivers quark distribution measurement, the study of these processes is also a interesting physics topic. Not only in 50-GeV and 30-GeV energies, but also in a lower energy, cross section measurements of charm production will be meaningful.

In order to measure the charm production, we should plan a open-geometry apparatus without tapered copper beam dump and/or Cu/C absorbers placed in the first magnet. It will improve the invariant mass resolution to identify charmonia. By installing electromagnetic calorimeters, we will be able to detect χ_c states of the charmonia. Precision tracking detectors, e.g. silicon detectors, will be useful to identify displaced vertex of the charmed mesons and improve the signal-to-noise ratio.

4.5 Gluon polarization in charmonia production with longitudinally polarized beam and target

Although we have already obtained the gluon polarization inside the proton from the RHIC experiments, it can only cover a limited high-x range. This causes an uncertainty

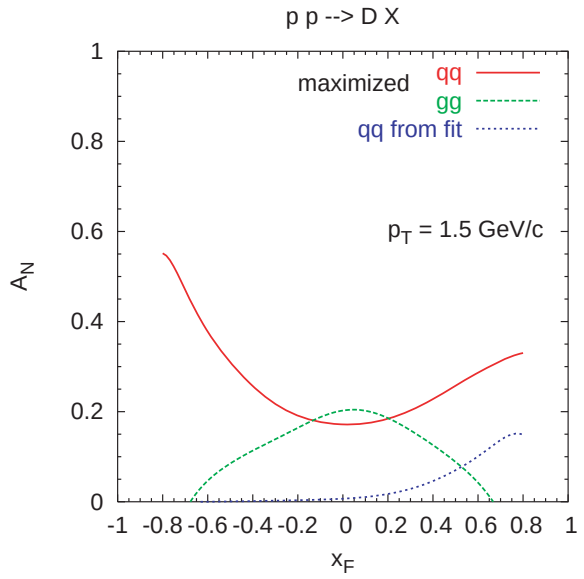

Figure 20: A_N of D-meson production by saturating the Sivers positivity bounds for quarks (maximized qq), for gluons (maximized gg), and by using the parametrizations of the quark Sivers function fit to the E704 data (qq from fit) [86, 87].

to evaluate ΔG, which requires an integration from $x = 0$ to $x = 1$. This proposed experiment offers a higher-x measurement of the gluon polarization.

The heavy-flavor production by the gluon-fusion process is one of the cleanest signal to investigate the gluon distribution inside the nucleon. In particular, χ_{c2} production is sensitive to the gluon polarization because it is produced mainly from helicity ± 2 states of the gluon-fusion process.

By installing electromagnetic calorimeters, we can detect χ_{c2} and distinguish it from χ_{c0} and χ_{c1}. It is difficult to distinguish $\chi_{c0}/\chi_{c1}/\chi_{c2}$ states in the collider experiments because of the low photon energy of the $\chi_c \to J/\psi + \gamma$ decay.

The angular distribution in the decay of the produced charmonium, $\chi_{c2} \to J/\psi + \gamma$, in the unpolarized case allows us to distinguish between the color singlet and color octet production mechanisms. Once the production mechanism is known, the angular distribution in the polarized case can be used to measure the gluon polarization [88].

5 Experimental Apparatus

5.1 Beam requirement

As illustrated in the previous sections, a 50-GeV proton beam is preferred, but fruitful results with a 30-GeV beam can be expected. The intensity of the proton beam is assumed to be 1×10^{12} /sec for the closed-geometry measurements. We understand that this intensity can be handled from the radiation-shielding point of view of the experimental hall. For the open-geometry measurements, the proton beam intensity should be from 1×10^{8} to 1×10^{10} /sec.

Since the spectrometer is designed so that the particles are analyzed by a vertically bending magnetic field, the vertical beam size and divergence at the experimental target is important. The actual numbers of the beam size and divergence should be discussed with the beamline experts of the J-PARC team, but we request that the vertical beam size be 1 cm or less. The horizontal beam size can be a few centimeters. We think the beam line considered in a Letter of Intent, "L14: Construction of a High Momentum Beam Line at the 50-GeV Proton Synchrotron", submittedto the J-PARC director about three years ago, is a good model of a beam line for our experiment.

The duty factor of the proton beam is another important factor. A high duty factor is preferable, but the intensity of 1×10^{12} /sec has to be guaranteed.

In addition, as illustrated in Section 4, rich physics can be foreseen by a polarized proton beam. While we understand that the initial goal of the J-PARC facility is to realize a high intensity unpolarized proton beam, a polarized proton beam is highly anticipated. Accelerator physicists have investigated a possibility of polarized proton acceleration at the J-PARC facility (eg. [89]). Their preliminary answer is that a polarized proton beam can be accelerated at the J-PARC facility with minimum additions of instruments, though further investigation in details should be necessary for its realization.

5.2 Targets

The experiment would use 20-inch long liquid hydrogen and deuterium targets, three nuclear targets of about 10 g/cm^2 thickness and a dummy liquid target cell. Details of the target design is to be discussed.

In addition, a polarized target will be developed and used for the measurement of the polarized target experiments mentioned in Sec.4.

5.3 Spectrometer design

The experimental apparatus is very similar to the one used in a series of experiment at Fermilab (E605, E772, E789, E866, and E906). Just after the experimental target, a large dipole magnet, whose bending plane is vertical, is located in order to focus the high momentum muons and defocus low momentum muons. A copper beam dump and hadron absorbers are inserted in the first dipole magnet. After the first magnet, position sensitive counters and a dipole magnet are located to measure momentum of the particles. In Fig. 21, the E866 spectrometer is schematically shown.

The Fermilab E906 experiment [44] is designed to use a 120-GeV proton beam from the Main Injector. In general, a spectrometer for a lower beam energy requires wider aperture of the spectrometer. Since the proposed experiment uses 50- and 30-GeV proton beams, a spectrometer for the experiment should have wider aperture than the E906 spectrometer. But to keep a similar total momentum kick with a realistic magnetic field and to realize the spectrometer with a realistic cost, the magnets of the same size as the E906 spectrometer have been selected, which has a sufficiently large acceptance as shown below. Horizontal and vertical sketches of the spectrometer are shown in Figs. 22 and 23 respectively.

The characteristics of the first magnet are listed in Tab. 1. This magnet can be constructed using a part of iron from existing magnets at Fermilab plus new coils. The design

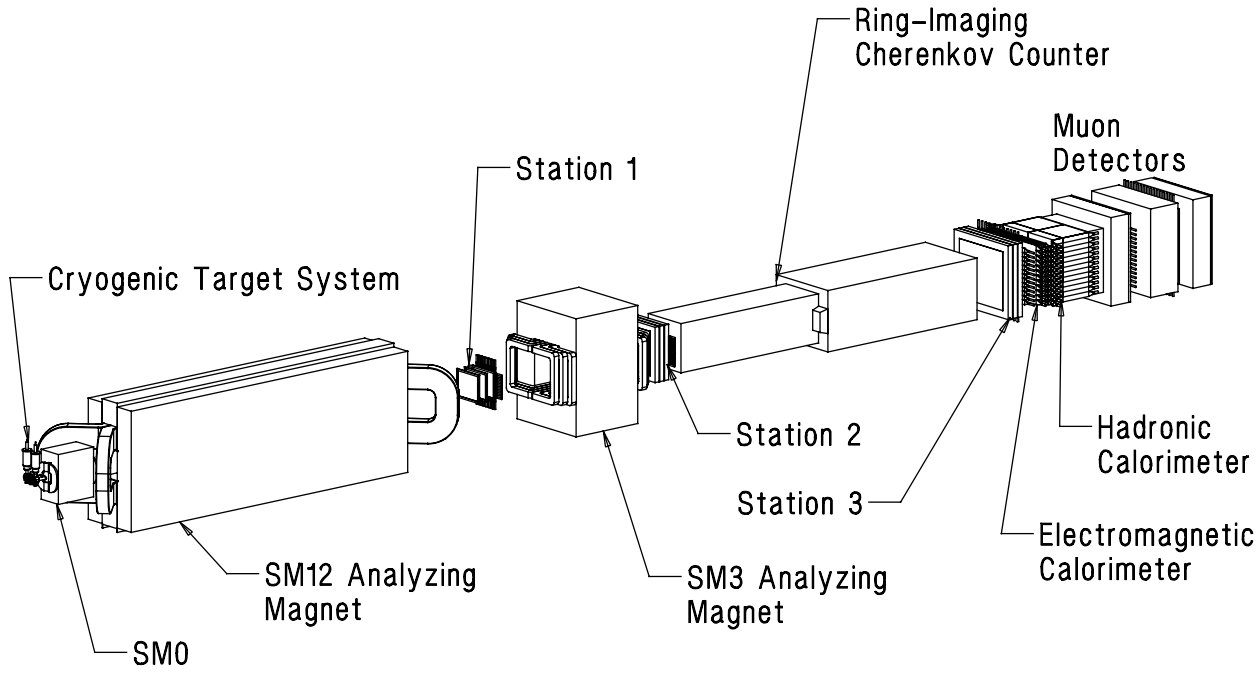

Figure 21: Schematic layout of the Meson-East focusing spectrometer at Fermilab.

of the copper beam dump including its cooling system and the detailed configuration of the hadron absorber is to be developed.

The second magnet has a smaller field integral but a larger aperture. The characteristics of the second magnet are shown in Tab. 2. This magnet is almost identical to the SM3 magnet which exists at the meson hall of Fermilab.

In Tab. 3, components of the experimental apparatus are listed.

A fast Monte-Carlo code, which takes into account the Drell-Yan cross section and the spectrometer configuration, has been used to estimate a statistical error for $\sigma(pd)/2\sigma(pp)$ shown in Figure 4. In order to estimate the yields and statistical errors, the following assumptions have been applied:

- The beam intensity is 1×10^{12} protons/(3 sec.).
- The net efficiency of data acquisition is 0.5.
- Data are taken for 60 days each for 50-cm long proton and deuteron targets.

The expected statistics are shown in Fig. 24 and the expected resolution is shown in Fig. 25. The performance of the spectrometer for $\vec{p}+\vec{p}$ measurement, nuclear dependence study of Drell-Yan, and J/Ψ production, has also been simulated and the results have been presented in the previous Sections.

5.4 Detector elements

According to the anticipated schedule, the Fermilab E906 experiment will be completed around 2010 and the equipments for E906 would becaom available. We expect to use

Table 1: Characteristics of the first magnet

Length	189 in
Width	95 in
Height	198 in
Vertical Aperture	48 in
Horizontal Aperture without inserts	26 in
Field Integral	8.14 T-m
Ampere-Turns	670230
Current	2394 Amp
Power	0.58 MW
Inlet Water Temperature	38 deg C
Temperature Rise	25 deg C
Water Flow	88 gal/min
Weight of Pole Inserts	9.5 t
Weight of Coild	19 t
Weight of Return Yoke	420 t
Total Weight	450 t

Table 2: Characteristics of the second magnet

Length	84 in
Width	135 in
Height	190 in
Vertical Aperture	96 in
Horizontal Aperture	50 in
Field Integral	1.65 T-m
Ampere-Turns	1010000
Current	980 Amp
Power	0.89 MW
Inlet Water Temperature	35 deg C
Temperature Rise	22 deg C
Water Flow	152 gal/min
Total Weight	220 t

Table 3: Components of the apparatus

Component	Subcomponent	Comments
Beam line		J-PARC
Target		J-PARC
M1	Coils	
	Inserts	
	Return Yoke	
	Assembly	
	Power Supplies	
M2	Repair Coil	
	Assembly	
Power Supplies		
Station 1 MWPC	Chambers	
	Electronics	
	Readout	
Station 1 Hodoscopes		
Station 2 DC	Chambers	
	Electronics	
	Readout	
Station 2 Hodoscopes		
Station 3 DC	Chambers	
	Electronics	
	Readout	
Station 3 Hodoscopes		
Station 4 Prop. Tubes	Chambers	
	Electronics	
	Readout	
Muon ID Wall	Assembly	
Gas System	Mixing	
	Distribution	
Station 4 Hodoscopes		
Trigger		
DAQ		
Analysis		

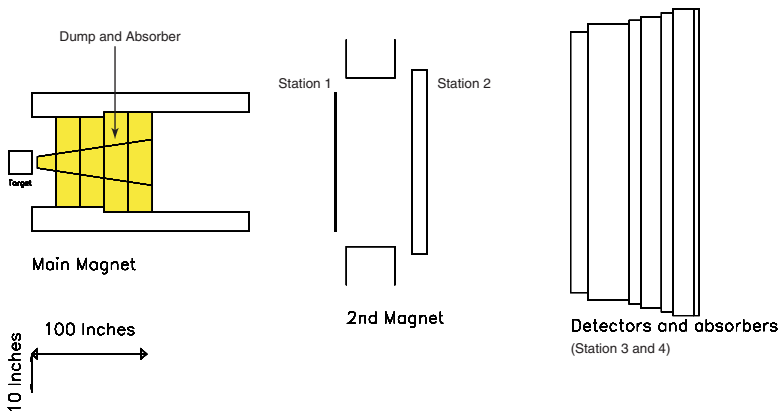

Figure 22: Schematic horizontal view of the prototype spectrometer.

many of the detectors and electronics from Fermilab E906 experiment for the proposed J-PARC experiment.

5.4.1 Tracking chambers

The high instantaneous rates at the station 1 lead us to plan for rates up to 100 MHz. We propose to use Multi-Wire-Proportional-Chambers with a 2 mm wire spacing. The first three planes would be MWPC's used in E605 with existing electronics. The stereo angles of the U and V wires are ± 14 degrees. The following 4 planes would use two existing E871 MWPC's, each covering half the x acceptance arranged with a 4" horizontal gap at x=0. The frames of the two chambers would overlap in this gap. While multiple scattering in the frames does not significantly deteriorate the resolution, this x=0 stripe avoids the highest count rate areas (at the maximum y). The stereo angle of these planes is ± 26 degrees. Existing E871 amplifier-discriminator-readout would be used. The readout would consist of 7000 channels of coincidence registers. All the electronics and readout currently exist at Fermilab.

Station 2 and 3 would use the existing E605/E772/E866 drift chamber stations 2 and 3. They are capable of 250 μm resolution with Ar/Ethane (50:50) gas. Existing preamplifiers and discriminators would be adequate. A 1700 channel multi-hit TDC system is required for good efficiency and rate capabilities.

Station 4 would be constructed of limited streamer tubes with a 1 cm pitch operated in proportional mode using existing amplifiers and discriminators from E866. Readout

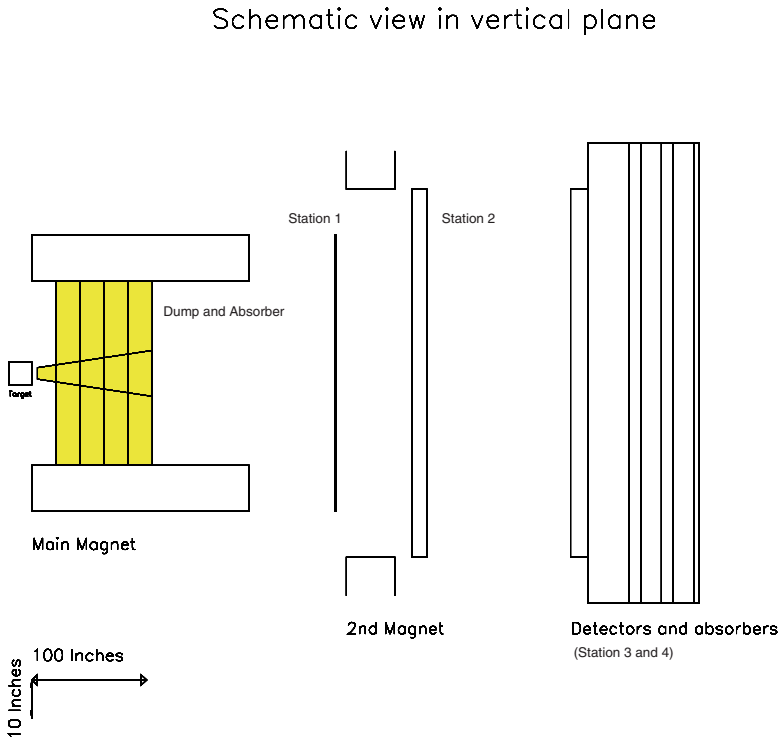

Figure 23: Schematic vertical view of the prototype spectrometer.

would be identical to the MWPC's and add 900 channels to the electronics and coincidence register total.

5.4.2 Scintillator hodoscopes

Scintillator hodoscope planes will provide the hit information for the hardware trigger system. There will be a total of eight planes, four to measure track y (bend plane) locations and four to measure track x locations. There will be a y hodoscope plane associated with each of the four detector stations - referred to as Y1, Y2, Y3, and Y4. They will contain 32 channels apiece, separated into 16 channels on the right side of the spectrometer ($x < 0$) and 16 channels on the left side ($x > 0$). These will be x hodoscope planes associated with detector stations 1 and 2, plus two additional planes as part of station 4 - referred to as X1, X2, X4A, and X4B. They will contain 32 channels apiece, separated into 16 channels for the lower half of the spectrometer ($y < 0$) and 16 channels for the upper half ($y > 0$). This segmentation will provide a logical division of each hodoscope plane into quadrants, allowing the trigger system to place tighter geometric constraints on the tracks.

All of the scintillators within a given y hodoscope plane will be the same size. The individual scintillators within hodoscope planes X4A and X4B will all the same angular size. In contrast, the four X1 and four X2 scintillators closest to $x = 0$ will subtend 1.5 times the angular range of the X4A and X4B scintillators and the remaining X1 and X2 scintillators. This segmentation minimizes the number of hodoscope channels in stations

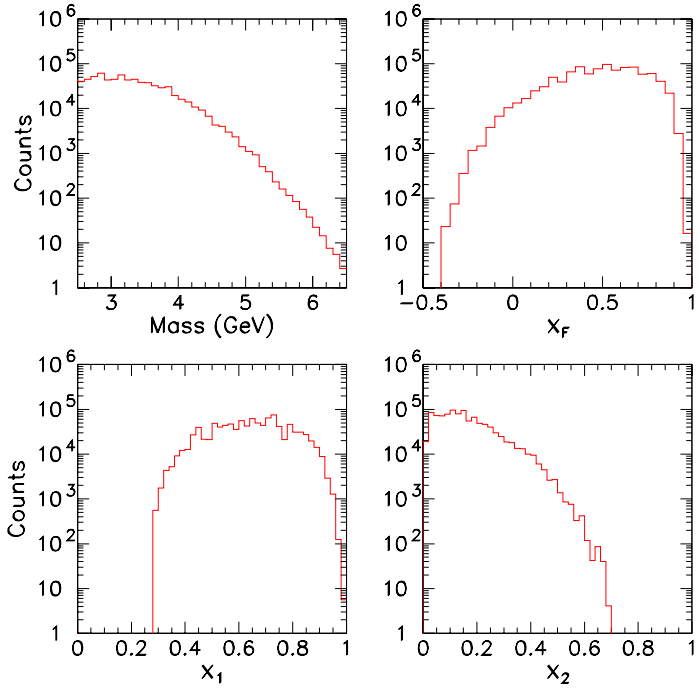

Figure 24: Expected statistics for mass, x_F, x_1, and x_2.

1 and 2 that may be in coincidence with given channels in X4A and X4B, after accounting for the multiple scattering of the muons through the various absorbers in the spectrometer.

5.4.3 Muon identification

Final muon identification is provided with a absorber wall, 81 cm of concrete followed by 92 cm of zinc and 10 cm of Pb, followed by 2 planes of streamer tubes and the X4A scintillators, then 92 cm of concrete followed by the Y4 and X4B scintillators and finally 92 cm of concrete followed by 2 planes of streamer tubes. The E866 muon identification walls provide enough material for the smaller wall in this experiment.

6 Summary

We propose to study dimuon production at J-PARC using 30 and 50 GeV proton beams on ^{2}H, ^{2}D and solid targets. A broad physics program addressing many aspects of the proton and nuclear quark/gluon structures can be pursued with unpolarized proton beams. The proposed apparatus will also be suitable for studying high-energy spin physics when polarzied proton beam becomes available at J-PARC. Many of the proponents of this proposal have extensive experiences in previous Fermilab dimuon experiments and the PHENIX experiment at RHIC. By utilizing some of the spectrometer and detector components from the Fermilab E906 dimuon experiment, the proposed experiment will be performed in a cost-effective fashion.

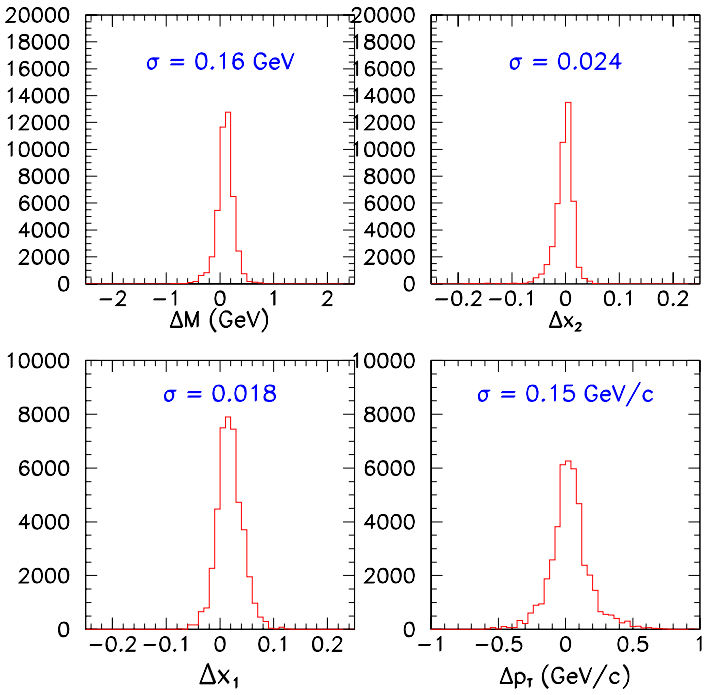

Figure 25: Expected resolution of mass, x_1, x_2, p_T.

References

[1] J. J. Aubert *et al.*, Phys. Lett. **B123**, 295 (1983).

[2] D. F. Geesaman, K. Saito, A. W. Thomas, Annu. Rev. Nucl. Part. Sci. **45**, 337 (1995).

[3] E. Hughes and R. Voss, Annu. Rev. Nucl. Part. Sci. **49**, 303 (1999).

[4] P. Amaudruz *et al.*, Phys. Rev. Lett. **66**, 2712 (1991); M.Arneodo *et al.*, Phys. Rev. D **55**, R1 (1994).

[5] K. Gottfried, Phys. Rev. Lett. **18**, 1174 (1967).

[6] S. D. Drell and T. M. Yan, Phys. Rev. Lett. **25**, 316 (1971).

[7] P. L. McGaughey, J. M. Moss and J. C. Peng, Annu. Rev. Nucl. Part. Sci. **49**, 217 (1999).

[8] E. A. Hawker *et al.*, Phys. Rev. Lett. **80**, 3715 (1998); R. S. Towell *et al.*, Phys. Rev. D **64**, 052002 (2001).

[9] J. C. Peng *et al.*, Phys. Rev. D **58**, 092004 (1998).

[10] D. A. Alde *et al.*, Phys. Rev. Lett. **64**, 2479 (1990).

[11] R. Baier *et al.*, Phys. Lett. **B345**, 277 (1995); Nucl. Phys. **B483**, 291 (1997); Nucl. Phys. **B484**, 265 (1997).

[12] R. G. Zakharov, JETP Letters **63**, 952 (1996); JETP Letters **65**, 615 (1997).

[13] L. D. Landau and I.Ya. Pomeranchuk, Dokl. Akad. Nauk SSSR **92**, 535 (1953); **92**, 735 (1953).

[14] A. B. Migdal, Phys. Rev. **103**, 1811 (1956).

[15] P. L. Anthony *et al.*, Phys. Rev. Lett. **75**, 1949 (1995); Phys. Rev. **D56**, 1373 (1997).

[16] M. A. Vasiliev *et al.*, Phys. Rev. Lett. **83**, 2304 (1999).

[17] M. B. Johnson *et al.*, Phys. Rev. Lett. **86**, 4483 (2001).

[18] A. Airapetian *et al.*, Eur. Phys. J. **C20**, 479 (2001).

[19] A. Airapetian *et al.*, Phys. Lett. **B577**, 37 (2003).

[20] G. T. Garvey and J. C. Peng, Phys. Rev. Lett. **90**, 092302 (2003).

[21] C. Gerschel and J. Hüfner, Annu. Rev. Nucl. Part. Sci. **49**, 255 (1999).

[22] R. Vogt, Phys. Rev. **C61**, 035203 (2000).

[23] T. Matsui and H. Satz, Phys. Lett. **B178**, 416 (1986).

[24] M. C. Abreu *et al.*, CERN-EP-2000-013 (2000).

[25] I. R. Kenyon, Rep. Prog. Phys. **45**, 1261 (1982).

[26] S. D. Ellis and W. J. Stirling, Phys. Lett. **B256**, 258 (1991).

[27] A. Baldit *et al.*, Phys. Lett. **B332**, 244 (1994).

[28] H. L. Lai *et al.*, Phys. Rev. **D55**, 1280 (1997).

[29] A. D. Martin, R. G. Roberts, W. J. Stirling, Phys. Lett. **B387**, 419 (1996).

[30] A. W. Thomas, Phys. Lett. **B126**, 97 (1983).

[31] J. D. Sullivan, Phys. Rev. **D5**, 1732 (1972).

[32] S. Kumano, Phys. Rev. **D43**, 3067 (1991); **D43**, 59 (1991); S. Kumano and J. T. Londergan, Phys. Rev. **D44**, 717 (1991).

[33] S. Kumano, Phys. Rept. **303**, 183 (1998).

[34] G. T. Garvey and J. C. Peng, Prog. Part. Nucl. Phys. **47**, 203 (2001).

[35] E. J. Eichten, I. Hinchliffe, C. Quigg, Phys. Rev. **D45**, 2269 (1992).

[36] T. P. Cheng and L. F. Li, Phys. Rev. Lett. **74**, 2872 (1995).

[37] A. Szczurek, A. Buchmans, A. Faessler, J. Phys. **C22**, 1741 (1996).

[38] M. Wakamatsu and T. Kubota, Phys. Rev. **D60**, 034020 (1999).

[39] P. V. Pobylitsa *et al.*, Phys. Rev. **D59**, 034024 (1999).

[40] D. I. Diakonov *et al.*, Phys. Rev. **D56**, 4069 (1997).

[41] S. Forte, Phys. Lett. **B224**, 189 (1989).

[42] S. Forte, Acta Phys. Polon. **B22**, 1065 (1991).

[43] W. Melnotchouk, J. Speth, and A. W. Thomas, Phys. Rev. **D59**, 014033 (1999).

[44] Proposal for Drell-Yan Measurements of Nucleon and Nuclear Structure with FNAL Main Injector, P906 Collaboration, `http://p25ext.lanl.gov/e866/papers/p906/proposal_final.ps`.

[45] R. Baier, D. Schiff and B. G. Zakharov, hep-ph/0002198 (2000).

[46] S. Gavin and J. Milana, Phys. Rev. Lett. **68**, 1834 (1992).

[47] S. J. Brodsky and P. Hoyer, Phys. Lett. **B298**, 165 (1993).

[48] F. E. Close, Phys. Lett. **B43**, 422 (1973).

[49] G. R. Farrar and D. R. Jackson, Phys. Rev. Lett. **35**, 1416 (1975).

[50] J. S. Webb *et al.*, hep-ex/0302019.

[51] C. H. Llewellyn-Smith, Phys. Lett. **B128**, 107 (1983).

[52] M. Ericson and A. W. Thomas, Phys. Lett. **B128**, 112 (1983).

[53] E. L. Berger, F. Coester and R. B. Wiringa, Phys. Rev. **D29**, 398 (1984).

[54] R. P. Bickerstaff *et al.*, Phys. Rev. Lett. **53**, 2531 (1984).

[55] V. R. Pandharipande *et al.*, Phys. Rev. **C49**, 789 (1994); A. Akmal *et al.*, Phys. Rev. **C56**, 2261 (1997).

[56] F. E. Close, R. L. Jaffe, R. G. Roberts and G. G. Ross, Phys. Rev. **D31**, 1004 (1985).

[57] C. S. Lam and W. K. Tung, Phys. Rev. **D21**, 2712 (1980).

[58] S. Falciano *et al.*, Z. Phys. **C31**, 513 (1986); M. Guanziroli *et al.*, Z. Phys. **C37**, 545 (1988).

[59] J. S. Conway *et al.*, Phys. Rev. **D39**, 92 (1989).

[60] A. Brandenburg *et al.*, Phys. Rev. Lett. **73**, 939 (1994).

[61] A. Branenburg *et al.*, Z. Phys. **C60**, 697 (1993).

[62] D. Boer, Phys. Rev. **D60**, 014012 (1999).

[63] M. H. Schub *et al.*, Phys. Rev. **D52**, 1307 (1995).

[64] M. S. Kowitt *et al.*, Phys. Rev. Lett. **72**, 1318 (1994).

[65] G. T. Bodwin, E. Braaten, and G. P. Lepage, Phys. Rev. **D51**, 1125 (1995).

[66] T. H. Chang *et al.*, Phys. Rev. Lett. **91**, 211901 (2003).

[67] M. Beneke and I. Z. Rothstein, Phys. Rev. **D54**, 2005 (1996).

[68] C. N. Brown *et al.*, Phys. Rev. Lett. **86**, 2529 (2001).

[69] M. J. Leitch *et al.*, Phys. Rev. Lett. **84**, 3256 (2000).

[70] X. Ji, J. W. Qiu, W. Vogelsang and F. Yuan, hep-ph/0602239; hep-ph/0604023.

[71] F. Yuan and W. Vogelsang, private communications.

[72] W. Vogelsang and F. Yuan, Phys. Rev. D **72**, 054028 (2005).

[73] V. Barone, A. Drago and P. G. Ratcliffe, Phys. Rept. **359**, 1 (2002).

[74] A. N. Sissakian, O. Y. Shevchenko, A. P. Nagaytsev and O. N. Ivanov, Phys. Rev. D **72**, 054027 (2005).

[75] B. Adeva *et al.*, Phys. Lett. **B420**, 180 (1998).

[76] K. Ackerstaff *et al.*, hep-ex/9906035 (1999).

[77] B. Dressler *et al.*, hep-ph/9909541 (1999).

[78] R. J. Fries and A. Schäfer, Phys. Lett. **B443**, 40 (1998).

[79] K. G. Boreskov and A. B. Kaidalov, Eur. Phys. J. **C10**, 143 (1999).

[80] T. Gehrmann and W. J. Stirling, Phys. Rev. **D53**, 6100 (1996).

[81] M. Glück, E. Reya, M. Stratmann and W. Vogelsang, Phys. Rev. **D53**, 4775 (1996).

[82] K. Goeke *et al.*, hep-ph/0003324 (2000).

[83] M. Glück, E. Reya and A. Vogt, Z. Phys. **C67**, 433 (1995).

[84] F. E. Close and D. Sivers, Phys. Rev. Lett. **39**, 1116 (1977).

[85] D. Adams *et al.*, Nucl. Instru. Meth. **A437**, 23 (1999).

[86] M. Anselmino, M. Boglione, U. D'Alesio, E. Leader and F. Murgia, Phys. Rev. D **70**, 074025 (2004).

[87] U. D'Alesio, private communications.

[88] R. L. Jaffe and D. Kharzeev, Phys. Lett. B **455**, 306 (1999).

[89] Tracking of polarized protons in the Main ring of the J-PARC accelerator facility, A. U. Luccio, KEK Report 2005-11 (2005).